EUROPEAN JOURNAL OF PURE AND APPLIED MATHEMATICS
2026, Vol. 19, Issue 2, Article Number 7733
ISSN 1307-5543 – ejpam.com
Published by New York Business Global

Quantitative Symmetry Profiling of Healthy and Diseased Leaves Using Logarithmic Coefficient Filters

Rabha W. Ibrahim[1,2,*], Dumitru Baleanu[3], Soheil Salahshour[4,5]

[1] *Department of Mathematics, Saveetha School of Engineering, Saveetha Institute of Medical and Technical Sciences SIMATS, Chennai, Tamil Nadu, 602105, India*
[2] *Information and Communication Technology Research Group, Scientific Research Center, Al-Ayen University, Thi-Qar, Nasiriyah 64001, Iraq*
[3] *Department of Computer Science and Mathematics, Lebanese American University, Beirut 11022801, Lebanon*
[4] *Advanced Computing Lab, Faculty of Engineering and Natural Sciences, Istanbul Okan University, 34959, Turkey*
[5] *Faculty of Engineering and Natural Sciences, Bahcesehir University, Istanbul, Turkey*

Abstract. This study develops a m-fold-symmetry driven framework for quantitative analysis and filtering of leaf images inspired by a generalized logarithmic expansion. Leaves of healthy plants exhibit strong bilateral or higher–order rotational symmetries, while diseased leaves show structural distortions that break these patterns. Motivated by analytic function theory, we interpret the logarithmic coefficients γ_n of a conformal mapping as angular harmonic amplitudes that encode local geometric balance. Starting from the polar representation of a leaf image, the log–intensity is expanded in angular Fourier series whose coefficients play the role of the γ_n. A general 3×3 window is then designed to project the local log–image onto the harmonics corresponding to multiples of a chosen symmetry order m. This window acts as a discrete filter that suppresses nonsymmetric components while preserving the dominant m-fold structure. Bilateral ($m = 2$) and higher–order windows are implemented and applied directly to grayscale images without prior segmentation. Experiments on a curated dataset of healthy and unhealthy leaves show that healthy samples achieve bilateral symmetry scores exceeding 0.94 with a clear dominance of the $m = 2$ harmonic, whereas diseased leaves exhibit reduced bilateral scores, weakened $m = 2$ energy, and elevated higher–order components. The proposed filter enhances the bilateral component, increases the separation between healthy and unhealthy score distributions, and remains robust to noise and illumination changes. The framework provides a mathematically interpretable tool for early detection of plant disease, automated health classification, and pre–processing for machine learning pipelines. Beyond plant pathology, the same 3×3 logarithmic window can be embedded in texture analysis, biomedical imaging, and any application requiring local symmetry enhancement or anomaly detection.

2020 Mathematics Subject Classifications: AMS classification codes

Key Words and Phrases: Logarithmic coefficients, carathfunction, herglotz representation, coefficient bounds, univalent function, analytic functions, geometric function theory, open unit disk, extremal problems, multiplier-defined subclasses.

---

1. Introduction

Geometric Function Theory (GFT) provides a rich analytic framework for studying the structural properties of planar domains through conformal mappings, univalent functions, and

*Corresponding Author.
DOI: https://doi.org/10.29020/nybg.ejpam.v19i2.7733

Email addresses: rabhaibrahim@yahoo.com (R.W. Ibrahim)
dumitru.baleanu@gmail.com (D. Baleanu), soheil.salahshour@okan.edu.tr (S.Salahshour)

their associated coefficient estimates. In the context of image processing, a grayscale or color image can be regarded as a sampled function on a planar domain, and local geometric features of the image correspond to the analytic and harmonic characteristics of an underlying mapping. The logarithmic coefficients γ_n appearing in the expansion $\log \frac{f(z)}{z}$ encode angular harmonics that capture symmetry, curvature, and distortion quantities that are directly relevant to texture analysis, shape recognition, and structural anomaly detection in images. By importing GFT tools such as subordination, coefficient bounds, and m–fold symmetrization into the design of local filters (e.g., the proposed 3×3 symmetry window), one obtains image operators that are mathematically interpretable and capable of enhancing or suppressing features associated with specific conformal or rotational symmetries. This connection allows classical GFT results to inform practical algorithms for denoising, disease detection, and pattern recognition in complex natural images such as plant leaves (see [1, 2]). The study of logarithmic coefficients for analytic and univalent functions has long been central to geometric function theory. In particular, classes defined via polynomial multipliers, such as [3–5]

$$\mathcal{F}(M) = \{f : \ f(0) = 0, \ f'(0) = 1, \ \Re\{M(z)f'(z)\} > 0, \ z \in \mathbb{D}\},$$

admit extremal problems that connect analytic coefficient bounds with potential-theoretic and variational methods [6–9]. Among these, skeletal representations offer unique benefits as well as certain drawbacks. Understanding that s-reps reside on a curved form space is essential to completing these computational tasks. Among the subclasses of $\mathcal{F}(M)$, those possessing additional rotational invariance, the so-called *m-fold symmetric classes*, play an important role [10–12]. A function f is said to be m-symmetric if it satisfies

$$f(\omega z) = \omega f(z), \qquad \forall\, \omega^m = 1,$$

which implies that its logarithmic expansion

$$\log \frac{f(z)}{z} = 2 \sum_{n \geq 1} \gamma_n z^n$$

has vanishing coefficients γ_n unless n is a multiple of m [13]. Pizer et al. [14, 15] examined both 2D and 3D objects with numerous potential representations. For more applications, we refere to [16–20]. Thus, in the m-symmetric class, the natural extremal problem is to determine sharp upper bounds for $|\gamma_{mj}|$. Classical results for the ambient (non-symmetric) classes establish that, for the canonical multipliers $M(z) = (1 - z)^2$ and $M(z) = 1 - z^2$, the sharp bounds are $|\gamma_n| \leq 1/n$ and $|\gamma_n| \leq 1/(2n)$, respectively. By restriction to the m-symmetric subclasses, one immediately deduces

$$|\gamma_{mj}| \leq \frac{1}{mj}, \qquad |\gamma_{mj}| \leq \frac{1}{2mj},$$

for the corresponding multiplier conditions. A fundamental question is whether these inequalities remain sharp in the symmetric setting, and if so, which functions attain them.

To better position the mathematical tools used in the subsequent sections, we emphasize that the proposed framework is not limited to classical geometric function theory, but can also be interpreted from an approximation-theoretic perspective. In particular, the logarithmic coefficients and the associated harmonic decomposition naturally align with expansions in orthogonal bases, where angular Fourier modes may be viewed as a special class of orthogonal polynomials on the unit circle. This viewpoint allows the filtering process to be understood as a projection onto symmetry-adapted subspaces, closely related to approximation operators and spectral truncation techniques. Such a connection enriches the theoretical foundation of the model and provides additional flexibility for extending the method using orthogonal polynomial systems

and related approximation tools (see, e.g., [21, 22]).
Recent developments show that the extremals in the symmetric class can be described through Schur–Carathéodory parameters and Blaschke product extremals adapted to the m-fold symmetry. In particular, the extremal Herglotz measures reduce to uniform orbit distributions on the unit circle, leading to explicit m-symmetric Blaschke extremals. These yield the same constants as in the non-symmetric case, but indexed by mj, thereby confirming the sharpness of the upper bounds within the symmetric subclasses. This framework provides a unified approach to extremal problems for logarithmic coefficients in symmetric classes, combining analytic, geometric, and potential-theoretic methods. To validate the proposed symmetry–filtering framework, we applied the logarithmic 3×3 window to a dataset of healthy and unhealthy leaf images. The filtered log-images reveal clear diagnostic contrasts: healthy leaves consistently achieve bilateral symmetry scores above 0.94 with a dominant $m = 2$ harmonic, while unhealthy leaves exhibit markedly lower bilateral scores, weakened $m = 2$ energy, and elevated higher-order contributions. Filtering in the logarithmic domain enhances structures, suppresses asymmetric noise, and increases the separation between healthy and diseased samples in quantitative symmetry metrics. These outcomes confirm that the analytic concepts developed in geometric function theory can be translated into robust, interpretable operators for real image processing tasks such as early disease detection and automated classification. Table 1 includes all the symbols that used in this effort.

Table 1: List of principal symbols used in the study.

Symbol	**Meaning**	**Remarks**
$f(z)$	Analytic or univalent function	$f(0) = 0,\ f'(0) = 1$
γ_n	Logarithmic coefficients	From $\log \frac{f(z)}{z} = 2\sum_{n\geq 1} \gamma_n z^n$
m	Symmetry order	$m = 2$ for bilateral, $m > 2$ for higher symmetries
$M(z)$	Auxiliary function $1 + \mu_1 z + \mu_2 z^2 + \cdots$	Defines generalized mapping kernel
K_m	3×3 local symmetry window	Used for image filtering in log-domain
H_j	Filter weight for harmonic j	$0 \leq H_j \leq 1$, controls low-pass strength
$J(x, y)$	Log-image intensity	$J = \log(\varepsilon + I)$
$\tilde{J}$	Filtered log-image	$\tilde{J} = K_m * J$
$I(r, \theta)$	Image intensity in polar coordinates	Used in harmonic decomposition
$\tilde{I}(r, \theta)$	Symmetry-filtered image	$\tilde{I} = \exp(\tilde{J}) - \varepsilon$
B_{iso}	Isotropic smoothing kernel	Stabilizes the 3×3 filter
$\alpha_c, \alpha_s, \beta$	Filter parameters	Control cosine/sine weights and smoothing
$\Re(\cdot)$	Real part of a complex quantity	Used in univalence and convexity conditions
$\Gamma_{q,\tau}(\alpha)$	(q, τ)–Gamma function	In extended versions of the model
$\text{supp}(f)$	Support of a function f	Region where f is nonzero

2. Upper Bounds of Symmetric Classes

In order to place our results in a broader analytic and potential-theoretic context, we introduce a generalized multiplier of arbitrary degree:

$$M(z) = 1 + \mu_1 z + \mu_2 z^2 + \cdots + \mu_n z^n, \qquad \mu_j \in \mathbb{R},\ n \geq 1.$$

This section is structured as follows. We begin by introducing the m-fold symmetric classes and associated multiplier conditions. We then present fundamental structural lemmas describing symmetry invariance and group symmetrization. These are followed by the main extremal results formulated in terms of Herglotz measures and external-field principles. Finally, we derive consequences for logarithmic coefficients that are essential for the subsequent image-processing framework.

Definition 1 (m-fold symmetric class). *Fix an integer $m \geq 2$. A function f analytic in $\mathbb{D}$ is called m-fold symmetric (and normalized) if*

$$f(0) = 0, \qquad f'(0) = 1, \qquad f(\omega z) = \omega\, f(z) \quad \textit{for all } \omega^m = 1.$$

Equivalently, f has the series form

$$f(z) = z + \sum_{j \geq 1} a_{mj+1}\, z^{mj+1},$$

so that $a_n = 0$ unless $n \equiv 1\,(\mathrm{mod}\ m)$.

Definition 2 (m-fold symmetric multiplier class). *Let M be a polynomial. Define $\mathcal{F}_m(M)$ to be the set of m-fold symmetric, normalized analytic functions f such that*

$$p(z) := M(z)\, f'(z) \in \mathcal{P} \quad \textit{and} \quad p(\omega z) = p(z) \quad \textit{for all } \omega^m = 1,$$

i.e. p is m-fold symmetric (its Herglotz measure is invariant under rotation by $2\pi/m$).

Remark 1. *The m-fold symmetry condition enforces a strong structural constraint on the analytic function, eliminating all coefficients except those aligned with the symmetry order. This sparsity plays a crucial role in both the theoretical extremal problems and the practical design of symmetry-selective filters in the image domain.*

Definition 3 (Real-coefficient subclass).

$$\mathcal{S}_{\mathbb{R}} := \Big\{ f(z) = z + \sum_{n \geq 2} a_n z^n : \ a_n \in \mathbb{R} \textit{ and } f \textit{ univalent in } \mathbb{D} \Big\}.$$

$$\mathcal{T} := \{ f \textit{ analytic in } \mathbb{D} : f(0) = 0, f'(0) = 1,\ \mathrm{Im}\, z \cdot \mathrm{Im}\, f(z) \geq 0 \}.$$

Example 1 (Odd schlicht class: $m = 2$). *$f(-z) = -f(z)$, so $f(z) = z + a_3 z^3 + a_5 z^5 + \cdots$ and $\log \frac{f(z)}{z} = 2(\gamma_2 z^2 + \gamma_4 z^4 + \cdots)$. Thus, $\gamma_{2k+1} = 0$. In the multiplier class $\mathcal{F}_2(M)$, the Herglotz measure is even, $d\nu(t) = d\nu(-t)$.*

Example 2 (m-fold Koebe-type extremal). *For $(1-z)^2$ within $\mathcal{S}_m$, the extremal is $f_m(z) = \frac{z}{(1-z^m)^{2/m}} = z + \frac{2}{m} z^{m+1} + \cdots$, which is m-fold symmetric and yields $2\gamma_{mj} = \frac{2}{mj}$, hence $\gamma_{mj} = \frac{1}{mj}$ and $\gamma_n = 0$ otherwise.*

Definition 4 (m-fold symmetry). *Fix $m \geq 2$. A normalized analytic function $f(z) = z + \sum_{n \geq 2} a_n z^n$ is called m-fold symmetric if*

$$f(\omega z) = \omega\, f(z) \quad \textit{for all } \omega^m = 1,$$

equivalently $a_n = 0$ unless $n \equiv 1 \pmod{m}$. In particular

$$\log \frac{f(z)}{z} = 2 \sum_{j \geq 1} \gamma_{mj}\, z^{mj} \quad (\gamma_n = 0 \textit{ if } n \not\equiv 0 \pmod{m}).$$

Definition 5 (Symmetric multiplier class)**.** *Let M be a polynomial and $m \geq 2$. Define $\mathcal{F}_m(M)$ as the set of m-fold symmetric, univalent f with*

$$f(0) = 0, \quad f'(0) = 1, \quad \Re\{M(z)f'(z)\} > 0 \quad \text{in } \mathbb{D},$$

and whose Carathéodory data $p(z) := M(z)f'(z)$ is m-fold symmetric:

$$p(\omega z) = p(z) \quad (\omega^m = 1).$$

Equivalently, in the Herglotz representation $p(z) = \int \frac{1+e^{it}z}{1-e^{it}z}\, d\nu(t)$ the probability measure ν is invariant under $t \mapsto t + 2\pi/m$.

Definition 6 (Support)**.** *Let $f : \mathbb{R} \to \mathbb{C}$ be a function. The* support *of f is*

$$\operatorname{supp}(f) := \overline{\{x \in \mathbb{R} : f(x) \neq 0\}}.$$

Similarly, if ν is a Borel measure on a topological space X, then

$$\operatorname{supp}(\nu) := \{x \in X : \nu(U) > 0 \text{ for every open neighborhood } U \ni x\}.$$

That is, the support of ν is the smallest closed set which carries all of the mass of ν.

Remark 2. *The notion of support plays a fundamental role in the analysis of Herglotz measures and extremal problems. It identifies the minimal set on which the measure is concentrated, thereby localizing the essential contribution to the analytic representation. In the context of symmetric classes, the support encodes the rotational structure and reduces extremal problems to finite orbit configurations. This is particularly important in Theorem 1, where optimal measures are shown to concentrate on maximizers of the external field. From an applied perspective, the support corresponds to dominant harmonic directions, providing a direct link between the abstract measure-theoretic formulation and the symmetry-selective filtering used in image processing.*

We have the following Lemmas.

Lemma 1 (Image of an m-fold symmetric analytic function is an m-fold symmetric domain)**.** *Let $m \in \mathbb{N}$ and set $\omega := e^{2\pi i/m}$. Suppose f is analytic in the unit disk $\mathbb{D}$ and has the m-fold symmetric expansion*

$$f(z) = z^m + \sum_{k=1}^{\infty} a_{mk+1}\, z^{mk+1}.$$

Then the image set $\Omega := f(\mathbb{D})$ is m-fold symmetric, i.e.

$$w \in \Omega \implies \omega w \in \Omega.$$

In particular, if f is univalent on $\mathbb{D}$, then Ω is an m-fold symmetric domain.

Proof. Let $\omega = e^{2\pi i/m}$. By the assumed form of f, we have for every $z \in \mathbb{D}$,

$$f(\omega z) = (\omega z)^m + \sum_{k=1}^{\infty} a_{mk+1}(\omega z)^{mk+1} = \omega^m z^m + \sum_{k=1}^{\infty} a_{mk+1}\, \omega^{mk+1} z^{mk+1}.$$

Since $\omega^m = 1$ and $\omega^{mk+1} = \omega^{mk}\omega = \omega$, this simplifies to

$$f(\omega z) = z^m + \omega \sum_{k=1}^{\infty} a_{mk+1} z^{mk+1} = \omega\Big(z^m + \sum_{k=1}^{\infty} a_{mk+1} z^{mk+1}\Big) = \omega\, f(z).$$

Now, fix any $w \in \Omega$. By definition of Ω, there exists $z \in \mathbb{D}$ with $f(z) = w$. Using the functional relation just proved,

$$\omega w = \omega f(z) = f(\omega z).$$

Because $|\omega z| = |z| < 1$, we have $\omega z \in \mathbb{D}$, hence $f(\omega z) \in f(\mathbb{D}) = \Omega$. Therefore $\omega w \in \Omega$, establishing the m-fold rotational invariance of Ω. If, additionally, f is univalent on $\mathbb{D}$, then Ω is a domain (open and simply connected as the conformal image of $\mathbb{D}$), and the invariance we just proved shows it is an m-fold symmetric domain.

Remark 3 (Equivalence with an equivariance relation)**.** *The series form of f above is equivalent to the equivariance identity*

$$f(\omega z) = \omega f(z) \qquad (z \in \mathbb{D},\ \omega^m = 1).$$

Indeed, the forward direction was shown in the proof. Conversely, if f is analytic and satisfies $f(\omega z) = \omega f(z)$, writing $f(z) = \sum_{n \geq 1} a_n z^n$ and comparing coefficients in

$$\sum_{n \geq 1} a_n \omega^n z^n \;=\; f(\omega z) \;=\; \omega f(z) \;=\; \sum_{n \geq 1} \omega a_n z^n,$$

we obtain $(\omega^n - \omega) a_n = 0$ for each n. Since $\omega \neq 0$, this forces $a_n = 0$ unless $\omega^{n-1} = 1$, i.e. $n \equiv 1 \pmod{m}$. Hence, $f(z) = \sum_{k \geq 0} a_{mk+1} z^{mk+1}$.
Lemma 1 shows that m-fold symmetry is not only an algebraic property of the function but also a geometric property of its image domain. This invariance under rotation provides a direct bridge between analytic function theory and geometric symmetry detection in images.

Example 3. *For $m = 3$, the function $f(z) = z^3 + a_4 z^4 + a_7 z^7 + \cdots$ satisfies $f(\omega z) = \omega f(z)$ with $\omega = e^{2\pi i/3}$, so $\Omega = f(\mathbb{D})$ is 3-fold symmetric. If f is univalent, Ω is a 3-fold symmetric domain.*

Lemma 2 (Group symmetrization)**.** *Fix an integer $m \geq 2$. Let ν be a Borel probability measure on the circle (identified with $[0, 2\pi)$ modulo 2π). For $\alpha \in \mathbb{R}$, let $R_\alpha : [0, 2\pi) \to [0, 2\pi)$ be the rotation $R_\alpha(t) := t + \alpha \pmod{2\pi}$, and denote by $R_\alpha \# \nu$ the pushforward of ν under R_α, i.e.*

$$(R_\alpha \# \nu)(E) := \nu\big(R_\alpha^{-1}(E)\big) \qquad \text{for Borel } E \subset [0, 2\pi).$$

Define the m-fold average

$$\overline{\nu} \;:=\; \frac{1}{m} \sum_{k=0}^{m-1} R_{2\pi k/m} \# \nu.$$

Then:

(i) *$\overline{\nu}$ is a Borel probability measure and is m-invariant, i.e.*

$$R_{2\pi/m} \# \overline{\nu} \;=\; \overline{\nu}.$$

(ii) *For every integer $\ell \in \mathbb{Z}$,*

$$\int_0^{2\pi} e^{i\ell t}\, d\overline{\nu}(t) \;=\; \frac{1}{m} \sum_{k=0}^{m-1} e^{i\ell\, 2\pi k/m} \int_0^{2\pi} e^{i\ell t}\, d\nu(t) \;=\; \begin{cases} \int_0^{2\pi} e^{i\ell t}\, d\nu(t), & \text{if } m \mid \ell, \\ 0, & \text{if } m \nmid \ell. \end{cases}$$

In particular, the Fourier moments at multiples of m are preserved, and all other moments vanish.

(iii) *Consequently, any functional that depends only on the moments* $\{\int e^{ijmt}\,d\nu(t)\}_{1\le j\le N}$ *(and their conjugates) has the same value at* ν *and* $\overline{\nu}$.

Proof. (i) Probability and invariance. Each pushforward $R_{2\pi k/m}\#\nu$ is a probability measure because

$$(R_{2\pi k/m}\#\nu)\big([0,2\pi)\big) = \nu\big(R^{-1}_{2\pi k/m}([0,2\pi))\big) = \nu([0,2\pi)) = 1.$$

Hence, their average $\overline{\nu}$ is also a probability measure. To prove m-invariance, use the composition property of pushforwards:

$$R_\alpha\#(R_\beta\#\nu) \;=\; R_{\alpha+\beta}\#\nu \qquad (\alpha,\beta\in\mathbb{R}).$$

Then, we get

$$R_{2\pi/m}\#\overline{\nu} = \frac{1}{m}\sum_{k=0}^{m-1} R_{2\pi/m}\#\big(R_{2\pi k/m}\#\nu\big) = \frac{1}{m}\sum_{k=0}^{m-1} R_{2\pi(k+1)/m}\#\nu.$$

Reindex with $j=k+1$; since indices are taken modulo m, $\{j : 0\le j\le m-1\} = \{k : 0\le k\le m-1\}$. Therefore

$$R_{2\pi/m}\#\overline{\nu} = \frac{1}{m}\sum_{j=0}^{m-1} R_{2\pi j/m}\#\nu = \overline{\nu}.$$

(ii) Fourier moments. For any bounded measurable φ one has the change-of-variables identity

$$\int \varphi(t)\,d(R_\alpha\#\nu)(t) = \int \varphi\big(R_\alpha(t)\big)\,d\nu(t).$$

Taking $\varphi(t) = e^{i\ell t}$ gives

$$\int e^{i\ell t}\,d(R_\alpha\#\nu)(t) = \int e^{i\ell(t+\alpha)}\,d\nu(t) = e^{i\ell\alpha}\int e^{i\ell t}\,d\nu(t).$$

Hence, we obtain

$$\int e^{i\ell t}\,d\overline{\nu}(t) = \frac{1}{m}\sum_{k=0}^{m-1}\int e^{i\ell t}\,d(R_{2\pi k/m}\#\nu)(t) = \frac{1}{m}\sum_{k=0}^{m-1} e^{i\ell\,2\pi k/m}\int e^{i\ell t}\,d\nu(t).$$

Set $\omega := e^{i2\pi\ell/m}$. Then

$$\frac{1}{m}\sum_{k=0}^{m-1}\omega^k = \begin{cases} 1, & \omega = 1 \;\; (\text{i.e., } m\mid\ell),\\ 0, & \omega\neq 1 \;\; (\text{i.e., } m\nmid\ell),\end{cases}$$

by the geometric-series formula $\sum_{k=0}^{m-1}\omega^k = (1-\omega^m)/(1-\omega)$ and the fact that $\omega^m = e^{i2\pi\ell} = 1$. This yields the stated dichotomy.

(iii) Functionals depending only on m-multiples. Let $m_{jm}(\nu) := \int e^{ijmt}\,d\nu(t)$. Part (ii) shows $m_{jm}(\overline{\nu}) = m_{jm}(\nu)$ for all j, while all other moments (nonmultiples of m) vanish for $\overline{\nu}$. Therefore, any functional that depends only on $\{m_m, m_{2m},\dots,m_{Nm}\}$ (and their conjugates) takes the same value at ν and $\overline{\nu}$.

Remark 4. *The symmetrization procedure eliminates all non-multiple Fourier modes while preserving the essential symmetric components. This mechanism is fundamental in reducing extremal problems to symmetric measures and is directly analogous to filtering operations that suppress asymmetric noise in image processing.*

Example 4 (Two-fold (odd) symmetrization: $m = 2$)**.** *Let ν be any probability measure on $[0, 2\pi)$ and let $R_\pi(t) := t + \pi$. The 2-fold symmetrization of ν is*

$$\overline{\nu} \;=\; \frac{1}{2}\big(\nu + R_\pi \# \nu\big),$$

where $(R_\pi \# \nu)(E) := \nu(R_\pi^{-1}(E))$ for Borel $E \subset [0, 2\pi)$. Then $\overline{\nu}$ is invariant under $t \mapsto t + \pi$ and, for every integer ℓ,

$$\int_0^{2\pi} e^{i\ell t}\, d\overline{\nu}(t) = \begin{cases} \displaystyle\int e^{i\ell t}\, d\nu(t), & \ell \text{ even}, \\ 0, & \ell \text{ odd}. \end{cases}$$

Proof. We compute the formula

$$\int e^{i\ell t}\, d(R_\pi \# \nu)(t) = \int e^{i\ell(t+\pi)}\, d\nu(t) = e^{i\ell\pi} \int e^{i\ell t}\, d\nu(t) = (-1)^\ell \int e^{i\ell t}\, d\nu(t).$$

Hence, we obtain

$$\int e^{i\ell t}\, d\overline{\nu}(t) = \frac{1}{2}\Big(1 + (-1)^\ell\Big) \int e^{i\ell t}\, d\nu(t),$$

which is the stated dichotomy. In particular, if p is the Carathéodory function with Herglotz measure ν, then the symmetrized measure $\overline{\nu}$ kills all odd *Fourier modes and preserves all* even *modes. Consequently, for any odd-symmetric normalized univalent f (i.e., $f(-z) = -f(z)$), one has*

$$\log \frac{f(z)}{z} = 2 \sum_{j \ge 1} \gamma_{2j}\, z^{2j}, \qquad \gamma_{2j+1} = 0,$$

and extremal problems involving γ_{2j} may be restricted to measures of the form $\overline{\nu} = \frac{1}{2}(\delta_\theta + \delta_{\theta+\pi})$ (with the same even moments as δ_θ).

Theorem 1 (Symmetric external-field extremals)**.** *Fix $m \ge 2$ and a polynomial multiplier M. Consider the class $\mathcal{F}_m(M)$ and a real C^1 functional*

$$\Phi(\nu) = F\big(m_m, m_{2m}, \ldots, m_{Nm}, \overline{m_m}, \ldots, \overline{m_{Nm}}\big), \quad m_{jm} := \int e^{ijmt}\, d\nu(t),$$

with any rotation-/phase-normalized side condition symmetric under $t \mapsto t + 2\pi/m$ (e.g. $\Re a_{m+1} > 0$). Suppose ν^* maximizes Φ over the Herglotz measures of $\mathcal{F}_m(M)$. Then

(i) *(*Reduction to symmetric measures*) By Lemma 2, there exists a maximizer that is m-invariant. In particular, we may assume ν^* is m-invariant.*

(ii) *(*External field and support*) The Euler–Lagrange external field*

$$G(t) = \Re\!\left(\sum_{j=1}^{N} \frac{\partial F}{\partial m_{jm}}(\nu^*)\, e^{ijmt} + \sum_{j=1}^{N} \frac{\partial F}{\partial \overline{m_{jm}}}(\nu^*)\, e^{-ijmt} \right)$$

is $2\pi/m$-periodic. There exists $\lambda_0 \in \mathbb{R}$ such that

$$G(t) \le \lambda_0 \ \text{ for all } t, \qquad G(t) = \lambda_0 \ \text{ for } t \in \sup p\nu^*.$$

Hence, $\operatorname{supp}(\nu^*)$ *is contained in the union of orbits of maximizers of G mod $2\pi/m$.*

(iii) *(*Orbit extremals*) If G has a unique maximizer modulo $2\pi/m$ at $t = \theta^* \in [0, 2\pi/m)$, then an extremal measure is the uniform m-orbit*

$$\nu^{\mathrm{orb}}_{\theta^*} := \frac{1}{m} \sum_{k=0}^{m-1} \delta_{\theta^*+2\pi k/m}.$$

Moreover, for every $j \geq 1$, $\int e^{ijmt}\, d\nu^{\mathrm{orb}}_{\theta^*} = e^{ijm\theta^*}$, so $\nu^{\mathrm{orb}}_{\theta^*}$ yields the same *relevant moments as the single atom δ_{θ^*}. Consequently, the two give the same value of Φ.*

Proof. (i) Apply Lemma 2 to any maximizer ν to get an m-invariant maximizer $\overline{\nu}$ with identical $(m, 2m, \ldots, Nm)$-moments and the same Φ-value; the side constraint is preserved by symmetry.
(ii) With ν^* m-invariant, vary by spikes $\nu_\varepsilon = (1-\varepsilon)\nu^* + \varepsilon\delta_t$. Since Φ depends only on m-multiples, the Gateaux derivative is

$$\frac{d}{d\varepsilon}\Big|_0 \Phi(\nu_\varepsilon) = \Re\Big(\sum_{j=1}^{N} c_{jm}\, e^{ijmt}\Big) - C = G(t) - \lambda_0,$$

with coefficients $c_{jm} = \partial F/\partial m_{jm}$ at ν^* and C is t-independent. Let ν^* be a maximizer and consider the spike variation $\nu_\varepsilon = (1-\varepsilon)\nu^* + \varepsilon\, \delta_t$. Assume the functional depends on moments up to order N:

$$\Phi(\nu) = F\big(m_1, \ldots, m_N, \overline{m_1}, \ldots, \overline{m_N}\big), \qquad m_k(\nu) := \int e^{ikt}\, d\nu(t).$$

Then, we get

$$\frac{d}{d\varepsilon}\Big|_0 m_k(\nu_\varepsilon) = e^{ikt} - m_k(\nu^*), \qquad \frac{d}{d\varepsilon}\Big|_0 \overline{m_k(\nu_\varepsilon)} = e^{-ikt} - \overline{m_k(\nu^*)}.$$

By the chain rule,

$$\begin{aligned}\frac{d}{d\varepsilon}\Big|_0 \Phi(\nu_\varepsilon) &= \sum_{k=1}^{N} \frac{\partial F}{\partial m_k}(\nu^*)\,(e^{ikt} - m_k(\nu^*)) + \sum_{k=1}^{N} \frac{\partial F}{\partial \overline{m_k}}(\nu^*)\,(e^{-ikt} - \overline{m_k(\nu^*)}) \\ &= \underbrace{\Re\Bigg(\sum_{k=1}^{N} \frac{\partial F}{\partial m_k}(\nu^*)\, e^{ikt} + \sum_{k=1}^{N} \frac{\partial F}{\partial \overline{m_k}}(\nu^*)\, e^{-ikt}\Bigg)}_{\text{depends on } t} - \underbrace{\Re\Bigg(\sum_{k=1}^{N} \frac{\partial F}{\partial m_k}(\nu^*)\, m_k(\nu^*) + \sum_{k=1}^{N} \frac{\partial F}{\partial \overline{m_k}}(\nu^*)\, \overline{m_k(\nu^*)}\Bigg)}_{C \text{ (independent of } t)}.\end{aligned}$$

Thus, the t-varying part is the displayed trigonometric polynomial, and C is exactly

$$C \;=\; \Re\Bigg(\sum_{k=1}^{N} \frac{\partial F}{\partial m_k}(\nu^*)\, m_k(\nu^*) + \sum_{k=1}^{N} \frac{\partial F}{\partial \overline{m_k}}(\nu^*)\, \overline{m_k(\nu^*)}\Bigg).$$

It does not depend on t because it only involves the *fixed* maximizer ν^*. Define the external-field potential

$$G(t) := \Re\Bigg(\sum_{k=1}^{N} \frac{\partial F}{\partial m_k}(\nu^*)\, e^{ikt} + \sum_{k=1}^{N} \frac{\partial F}{\partial \overline{m_k}}(\nu^*)\, e^{-ikt}\Bigg).$$

Then, we have

$$\frac{d}{d\varepsilon}\Big|_0 \Phi(\nu_\varepsilon) = G(t) - C.$$

The necessary optimality (no profitable transport of mass) is $G(t) \le \lambda_0$ for all t with equality on $\operatorname{supp}\nu^*$, where we simply set $\lambda_0 := C$. Hence, the contact C level in the Euler–Lagrange condition. If a side constraint is active (e.g. $a_2 = \Re m_1 - \mu_1/2 = 0$), use the Lagrangian

$$\mathcal{L}(\nu) = \Phi(\nu) \; - \; \lambda_1\Big(\tfrac{\mu_1}{2} - \Re m_1(\nu)\Big), \qquad \lambda_1 \ge 0.$$

Its variation adds $\lambda_1(\cos t - \mu_1/2)$ to $G(t)$ and adds the *constant* $\lambda_1\big(\Re m_1(\nu^*) - \frac{\mu_1}{2}\big)$ to C. At an active optimum $\Re m_1(\nu^*) = \mu_1/2$, so this extra constant vanishes. Therefore, the verified form is

$$G(t) = \Re\Big(\sum_k \partial_{m_k} F\, e^{ikt} + \partial_{\overline{m_k}} F\, e^{-ikt}\Big) \; + \; \lambda_1\big(\cos t - \tfrac{\mu_1}{2}\big), \qquad \lambda_0 = C.$$

m**-fold symmetric variant.** If Φ depends only on the multiples $m, 2m, \dots, Nm$, replace k by jm everywhere; the same calculation gives

$$C = \Re\left(\sum_{j=1}^{N} \frac{\partial F}{\partial m_{jm}}(\nu^*)\, m_{jm}(\nu^*) + \sum_{j=1}^{N} \frac{\partial F}{\partial \overline{m_{jm}}}(\nu^*)\, \overline{m_{jm}(\nu^*)}\right),$$

and

$$G(t) = \Re\left(\sum_{j=1}^{N} \frac{\partial F}{\partial m_{jm}}(\nu^*)\, e^{ijmt} + \sum_{j=1}^{N} \frac{\partial F}{\partial \overline{m_{jm}}}(\nu^*)\, e^{-ijmt}\right),$$

which is $2\pi/m$-periodic. Again, $\lambda_0 = C$. The standard Frostman–Euler–Lagrange condition gives $G \le \lambda_0$ with equality on $\operatorname{supp}(\nu^*)$. Periodicity $G(t + 2\pi/m) = G(t)$ is immediate.
(iii) If G has a unique maximizer modulo $2\pi/m$ at θ^*, then all points in the orbit $\theta^* + 2\pi k/m$ are maximizers. Any probability measure supported on that orbit with *any* weights has, for each $\ell = jm$,

$$\int e^{i\ell t}\, d\nu(t) = \sum_{k=0}^{m-1} w_k\, e^{i\ell(\theta^* + 2\pi k/m)} = e^{i\ell\theta^*} \sum_{k=0}^{m-1} w_k\, e^{i2\pi jk} = e^{i\ell\theta^*},$$

since $e^{i2\pi jk} = 1$. Thus, all such measures share the same relevant moments as δ_{θ^*}; choosing the *uniform* orbit ensures m-invariance of p and membership in $\mathcal{F}_m(M)$. Hence, $\nu_{\theta^*}^{\mathrm{orb}}$ is extremal and attains the same value of Φ as δ_{θ^*}.

Remark 5. *Theorem 1 provides a structural characterization of extremal measures via uniform m-orbits. This result significantly simplifies the optimization problem, reducing it to a finite-dimensional setting and revealing that symmetric extremals are sufficient to capture the maximal behavior of logarithmic coefficients.*

Corollary 1 (Reduction for $|\gamma_{mj}|$)**.** *Fix $m \ge 2$ and a polynomial multiplier M. Consider the symmetric multiplier class $\mathcal{F}_m(M)$, i.e., the set of m-fold symmetric, normalized univalent functions f in $\mathbb{D}$ with*

$$f(0) = 0, \quad f'(0) = 1, \quad \Re\{M(z)f'(z)\} > 0,$$

and whose Carathéodory data $p(z) := M(z)f'(z)$ is m-fold symmetric (equivalently, its Herglotz measure ν is invariant under $t \mapsto t + \frac{2\pi}{m}$). Then:

(a) *For every $f \in \mathcal{F}_m(M)$ one has*

$$\log\frac{f(z)}{z} \; = \; 2\sum_{j\ge 1} \gamma_{mj}\, z^{mj} \qquad \big(\textit{in particular } \gamma_n = 0 \textit{ if } n \not\equiv 0 \pmod m\big).$$

(b) *Let $j \geq 1$ be fixed and let $\Phi(\nu) := \pm \Re\big(e^{-i\phi}\gamma_{mj}(\nu)\big)$ for some $\phi \in \mathbb{R}$ (chosen so that $\max|\gamma_{mj}| = \max_\phi \max \Phi$). Over the feasible Herglotz measures of $\mathcal{F}_m(M)$, the supremum of Φ is attained by a* uniform m-orbit *measure*

$$\nu_{\theta^*}^{\mathrm{orb}} \;=\; \frac{1}{m}\sum_{k=0}^{m-1} \delta_{\theta^* + \frac{2\pi k}{m}} \quad \text{for some } \theta^* \in [0, 2\pi/m),$$

and its value equals the value of Φ at the single atom δ_{θ^*}:

$$\Phi(\nu_{\theta^*}^{\mathrm{orb}}) = \Phi(\delta_{\theta^*}).$$

Consequently,

$$\sup_{\nu \in \mathcal{F}_m(M)} |\gamma_{mj}(\nu)| \;=\; \sup_{\theta \in [0, 2\pi/m)} |\gamma_{mj}(\delta_\theta)|,$$

and for feasibility inside $\mathcal{F}_m(M)$ one may replace δ_θ by $\nu_\theta^{\mathrm{orb}}$ without changing the value of $|\gamma_{mj}|$.

Proof. (a) Sparsity. If f is m-fold symmetric, then $f(\omega z) = \omega f(z)$ for all m-th roots ω. Divide by ωz to get $\dfrac{f(\omega z)}{\omega z} = \dfrac{f(z)}{z}$, take logarithms, and expand in a power series:

$$\log \frac{f(\omega z)}{\omega z} = \log \frac{f(z)}{z}.$$

Comparing coefficients of z^n and using $\omega^n \neq 1$ unless $m \mid n$, we conclude that the coefficient of z^n must vanish unless n is a multiple of m. Hence, $\log \frac{f(z)}{z} = 2\sum_{j\geq 1} \gamma_{mj} z^{mj}$.
(b) Orbit reduction and attainment. Let ν be any feasible Herglotz measure for $\mathcal{F}_m(M)$. By the *group symmetrization* Lemma,

$$\overline{\nu} := \frac{1}{m}\sum_{k=0}^{m-1} R_{2\pi k/m} \# \nu \quad \big(R_\alpha(t) := t + \alpha\big)$$

is m-invariant and satisfies

$$\int e^{i\ell t}\, d\overline{\nu}(t) = \begin{cases} \displaystyle\int e^{i\ell t}\, d\nu(t), & \ell \equiv 0 \pmod{m}, \\ 0, & \ell \not\equiv 0 \pmod{m}. \end{cases}$$

By part (a), γ_{mj} depends only on the moments $m_m, m_{2m}, \dots, m_{jm}$ (multiples of m). Therefore, $\gamma_{mj}(\overline{\nu}) = \gamma_{mj}(\nu)$ and hence $\Phi(\overline{\nu}) = \Phi(\nu)$. It follows that the supremum of Φ over $\mathcal{F}_m(M)$ may be taken over the smaller set of m-invariant (i.e., symmetric) measures. Now apply the *symmetric external-field* theorem (Theorem 1) to Φ: for any maximizer ν^* there is an external-field trigonometric polynomial

$$G(t) = \Re\Big(\sum_{r=1}^{R} c_{rm}\, e^{irmt}\Big)$$

($2\pi/m$-periodic) such that $G(t) \leq \lambda_0$ for all t, with equality on $\mathrm{supp}(\nu^*)$. In particular, any point t in the orbit $\{\theta + 2\pi k/m\}$ of a maximizer θ of G is again a maximizer of G. If G has a *unique* maximizer modulo $2\pi/m$ at $\theta^* \in [0, 2\pi/m)$, then Theorem 1(iii) shows that the uniform orbit $\nu_{\theta^*}^{\mathrm{orb}} = \frac{1}{m}\sum_{k=0}^{m-1} \delta_{\theta^* + 2\pi k/m}$ is extremal. Even if G has several maximizing orbits, any probability measure supported on a union of maximizing orbits is extremal, so in particular at least one uniform orbit measure is extremal. Finally, for each $r \geq 1$,

$$\int e^{irmt}\, d\nu_{\theta^*}^{\mathrm{orb}}(t) = \frac{1}{m}\sum_{k=0}^{m-1} e^{irm(\theta^* + 2\pi k/m)} = e^{irm\theta^*} \cdot \frac{1}{m}\sum_{k=0}^{m-1} 1 = e^{irm\theta^*}.$$

Thus, the *relevant* moments (m-multiples) of $\nu_{\theta^*}^{\mathrm{orb}}$ *coincide* with those of the single atom δ_{θ^*}:

$$\int e^{irmt}\, d\nu_{\theta^*}^{\mathrm{orb}}(t) = \int e^{irmt}\, d\delta_{\theta^*}(t) = e^{irm\theta^*} \qquad (r = 1, \dots, j).$$

Since γ_{mj} is a smooth function of these moments only, we get $\gamma_{mj}(\nu_{\theta^*}^{\mathrm{orb}}) = \gamma_{mj}(\delta_{\theta^*})$ and hence, we get $\Phi(\nu_{\theta^*}^{\mathrm{orb}}) = \Phi(\delta_{\theta^*})$. Therefore, we obtain

$$\sup_{\nu \in \mathcal{F}_m(M)} \Phi(\nu) = \sup_{\theta \in [0,2\pi/m)} \Phi(\nu_\theta^{\mathrm{orb}}) = \sup_{\theta \in [0,2\pi/m)} \Phi(\delta_\theta),$$

and taking the outer supremum over the phase ϕ yields the stated reduction for $|\gamma_{mj}|$.

Remark 6. *This corollary establishes that the extremal behavior of logarithmic coefficients in symmetric classes can be fully understood through orbit measures. Consequently, the analysis of coefficient bounds aligns naturally with harmonic decomposition, which underpins the proposed filtering framework.*

Example 5 (Odd class $m = 2$ with $(1-z)^2$)**.** *In the $m = 2$ subclass of the convex class $M(z) = (1-z)^2$, take $f_2(z) = \dfrac{z}{(1-z^2)^1} = z + z^3 + z^5 + \cdots$. Then*

$$\log \frac{f_2(z)}{z} = -\log(1 - z^2) = \sum_{j \ge 1} \frac{z^{2j}}{j},$$

so $2\gamma_{2j} = \dfrac{2}{2j} \Rightarrow \gamma_{2j} = \dfrac{1}{2j}$, while $\gamma_{2j+1} = 0$. Theorem 1 says any sharp bound for $|\gamma_{2j}|$ is realized by either a single atom δ_θ or its symmetric 2-orbit $\frac{1}{2}(\delta_\theta + \delta_{\theta+\pi})$, which have identical even moments.

Theorem 2 (Distortion–Cauchy bound for the symmetric subsequence $|\gamma_{mj}|$)**.** *Let $m \ge 2$ and let M be a polynomial with no zeros in $\mathbb{D}$. Suppose f is m-fold symmetric, analytic and univalent in $\mathbb{D}$, normalized by $f(0) = 0$, $f'(0) = 1$, and*

$$\Re\{M(z) f'(z)\} > 0 \quad (z \in \mathbb{D}).$$

Write $\log\big(f(z)/z\big) = 2\sum_{n \ge 1} \gamma_n z^n$; then $\gamma_n = 0$ unless n is a multiple of m. Define for $t \in (0,1)$ the extremal moduli

$$m_M(t) := \min_{|z|=t} |M(z)|, \qquad M^*(t) := \max_{|z|=t} |M(z)|,$$

and the radial distortion integrals

$$L_M(r) := \int_0^r \frac{1-t}{1+t} \frac{dt}{M^*(t)}, \qquad I_M(r) := \int_0^r \frac{1+t}{1-t} \frac{dt}{m_M(t)} \qquad (0 < r < 1).$$

Then for every $j \ge 1$,

$$|\gamma_{mj}| \;\le\; \inf_{0<r<1} \frac{1}{2\, r^{mj}} \max\Big\{ \log \frac{I_M(r)}{r},\; \log \frac{r}{L_M(r)} \Big\}. \tag{1}$$

Proof. Because f is m-fold symmetric, we can write $f(z) = z\, F(z^m)$ with F analytic in $\mathbb{D}$ and $F(0) = 1$. Let $u = z^m$. Then

$$\log \frac{f(z)}{z} = \log F(z^m) =: H(u) = 2 \sum_{j \ge 1} \Gamma_j\, u^j,$$

so that $\gamma_{mj} = \Gamma_j$ for every $j \geq 1$. Fix $s \in (0,1)$ and set $r = s^{1/m}$. On $|u| = s$ we can parametrize by $u = r^m e^{im\theta}$ and $z = re^{i\theta}$; then

$$|F(u)| = \left|\frac{f(z)}{z}\right| \leq \frac{\sup_{|z|=r}|f(z)|}{r} \ \leq \ \frac{I_M(r)}{r}$$

by the same upper distortion bound used in the nonsymmetric case (obtained from $|f'|$ via $p(z) = M(z)f'(z) \in \mathcal{P}$). Similarly,

$$|F(u)| \geq \frac{\inf_{|z|=r}|f(z)|}{r} \ \geq \ \frac{L_M(r)}{r}.$$

Hence, on $|u| = s$,

$$\| \Re H \|_{L^\infty} \ \leq \ \max\Big\{ \log \frac{I_M(r)}{r}, \ \log \frac{r}{L_M(r)} \Big\}.$$

Cauchy's estimate for the u-series $H(u) = 2\sum_{j\geq 1}\Gamma_j u^j$ gives

$$|\Gamma_j| \leq \frac{1}{2\,s^j} \,\| \Re H \|_{L^\infty(|u|=s)}.$$

Recalling $s = r^m$ and $\Gamma_j = \gamma_{mj}$ yields (1).

Corollary 2 (Sharp constants in two canonical classes)**.** *Fix $m \geq 2$. Consider the m-fold symmetric multiplier classes $\mathcal{F}_m(M)$ associated with the two multipliers*

$$M_1(z) = (1-z)^2, \qquad M_2(z) = 1 - z^2.$$

Let f be normalized, analytic, univalent in $\mathbb{D}$, with $\Re\{M_j(z)f'(z)\} > 0$ and m-fold symmetric. Writing

$$\log \frac{f(z)}{z} = 2\sum_{n\geq 1}\gamma_n z^n,$$

one has $\gamma_n = 0$ unless $m \mid n$, and for every $j \geq 1$ the sharp bounds are

$$|\gamma_{mj}| \leq \frac{1}{mj} \quad \textit{for } M_1(z) = (1-z)^2, \qquad |\gamma_{mj}| \leq \frac{1}{2\,mj} \quad \textit{for } M_2(z) = 1 - z^2,$$

and both are attained. Hence

$$\sup_{f\in\mathcal{F}_m(M_1)} |\gamma_{mj}| = \frac{1}{mj}, \qquad \sup_{f\in\mathcal{F}_m(M_2)} |\gamma_{mj}| = \frac{1}{2\,mj}.$$

Proof. Step 1: Sharp constants in the ambient (non-symmetric) classes. Let $\mathcal{F}(M)$ denote the (non-symmetric) multiplier class

$$\mathcal{F}(M) = \Big\{ f : \ f(0) = 0, \ f'(0) = 1, \ \Re\{M(z)f'(z)\} > 0 \text{ in } \mathbb{D} \Big\}.$$

It is classical (and also follows from the one-point Herglotz extremals developed earlier) that for all $n \geq 1$,

$$\sup_{f\in\mathcal{F}((1-z)^2)} |\gamma_n| = \frac{1}{n}, \qquad \sup_{f\in\mathcal{F}(1-z^2)} |\gamma_n| = \frac{1}{2n}. \tag{2}$$

Indeed, the functions

$$f^{(1)}(z) = \frac{z}{(1-z)^2} \quad \text{and} \quad f^{(2)}(z) = \frac{z}{1-z}$$

belong respectively to $\mathcal{F}((1-z)^2)$ and $\mathcal{F}(1-z^2)$ because

$$(1-z)^2 f^{(1)\prime}(z) = \frac{1+z}{1-z} \in \mathcal{P}, \qquad (1-z^2) f^{(2)\prime}(z) = \frac{1+z}{1-z} \in \mathcal{P},$$

where $\mathcal{P}$ is the Carathéodory class. Moreover,

$$\log \frac{f^{(1)}(z)}{z} = -2\log(1-z) = 2\sum_{n\geq 1} \frac{z^n}{n} \;\Rightarrow\; \gamma_n = \frac{1}{n},$$

and

$$\log \frac{f^{(2)}(z)}{z} = -\log(1-z) = \sum_{n\geq 1} \frac{z^n}{n} \;\Rightarrow\; \gamma_n = \frac{1}{2n}.$$

Thus (5) holds with equality achieved by $f^{(1)}$ and $f^{(2)}$.

Step 2: Upper bounds in the symmetric subclasses. Let $\mathcal{F}_m(M) \subset \mathcal{F}(M)$ denote the m-fold symmetric subclass, i.e., $f(\omega z) = \omega f(z)$ for all m-th roots ω, and $p(z) := M(z)f'(z) \in \mathcal{P}$ is compatible with that symmetry (equivalently, the Herglotz measure is $2\pi/m$-periodic). For any $f \in \mathcal{F}_m(M)$ we still have $f \in \mathcal{F}(M)$, hence by (5) with $n = mj$,

$$|\gamma_{mj}(f)| \leq \sup_{g\in\mathcal{F}(M)} |\gamma_{mj}(g)| = \begin{cases} \frac{1}{mj}, & M = (1-z)^2, \\ \frac{1}{2\,mj}, & M = 1-z^2. \end{cases}$$

Taking the supremum over $f \in \mathcal{F}_m(M)$ gives the desired *upper* bounds in the symmetric subclasses.

Step 3: Attainment in the symmetric subclasses via group symmetrization. We now show these upper bounds are attained inside $\mathcal{F}_m(M)$. Fix $M \in \{(1-z)^2,\ 1-z^2\}$ and set $\nu^* := \delta_0$, the Dirac mass at 0. Let $p^*(z)$ be its Carathéodory function:

$$p^*(z) = \frac{1+z}{1-z} \in \mathcal{P}.$$

Let $f^* \in \mathcal{F}(M)$ be the unique normalized solution of

$$M(z)\, f^{*\prime}(z) = p^*(z), \qquad f^*(0) = 0.$$

As shown in Step 1, f^* is precisely $f^{(1)}$ when $M = (1-z)^2$ and $f^{(2)}$ when $M = 1-z^2$; in both cases, the n-th logarithmic coefficients satisfy the sharp equalities of (5). To enforce m-fold symmetry without changing the *relevant* moments, apply the m-fold averaging (group symmetrization) to ν^*:

$$\overline{\nu} := \frac{1}{m}\sum_{k=0}^{m-1} R_{2\pi k/m}\#\nu^* = \frac{1}{m}\sum_{k=0}^{m-1} \delta_{2\pi k/m},$$

which is a probability measure invariant under $t \mapsto t + 2\pi/m$. By Lemma 2 (group symmetrization), its Fourier moments satisfy

$$\int e^{i\ell t}\, d\overline{\nu}(t) = \begin{cases} \displaystyle\int e^{i\ell t}\, d\nu^*(t) = 1, & \ell \equiv 0 \pmod{m}, \\ 0, & \ell \not\equiv 0 \pmod{m}. \end{cases}$$

In particular, for each $j \geq 1$,

$$\int e^{imjt}\, d\overline{\nu}(t) = \int e^{imjt}\, d\nu^*(t) = 1.$$

Let $\overline{p}(z)$ be the Carathéodory function corresponding to $\overline{\nu}$ and let $\overline{f} \in \mathcal{F}(M)$ be the normalized solution of

$$M(z)\,\overline{f}'(z) = \overline{p}(z), \qquad \overline{f}(0) = 0.$$

By construction, $\overline{p}$ (hence $\overline{f}$) is m-fold symmetric, so $\overline{f} \in \mathcal{F}_m(M)$. Moreover, the logarithmic coefficients of $\overline{f}$ and f^* agree on the m-grid:

$$\gamma_{mj}(\overline{f}) = \gamma_{mj}(f^*) \qquad (j \geq 1),$$

because each γ_{mj} is a smooth polynomial function of the moments $\big\{\int e^{i\ell t}\,d\nu(t)\big\}_{\ell\leq mj}$ and the two measures $\overline{\nu}$ and ν^* have identical moments at all multiples of m (and the non-multiples play no role for γ_{mj} in the m-fold symmetric setting). Consequently,

$$|\gamma_{mj}(\overline{f})| = \begin{cases} \frac{1}{mj}, & M = (1-z)^2, \\ \frac{1}{2\,mj}, & M = 1 - z^2, \end{cases}$$

which matches the upper bounds of Step 2. Thus, the bounds are *sharp* and are attained by $\overline{f} \in \mathcal{F}_m(M)$.

Remark 7 (Relation to capacity preservation and the external-field method)**.** *The capacity/distortion envelope used in your external-field analysis is encoded precisely by L_M and I_M. The* Distortion–Cauchy *bound* (1) *is therefore driven by the* same *envelope for a general polynomial M; it gives a robust, explicit upper bound for $|\gamma_{mj}|$ for all j. When the external-field problem has a one-point extremal (as in the corollary), the capacity method recovers the* sharp *constants* $1/(mj)$ *and* $1/(2mj)$*. For mixed-sign or higher-degree multipliers, the external-field approach can still sharpen* (1) *by locating the exact maximizing orbit, whereas* (1) *remains a clean universal upper bound with the correct $O(1/(mj))$ decay once the radius is optimized.*

Example 6 (Detailed sharp example for $M(z) = 1 - z^2$ in the $m = 2$ (odd) class)**.** *Let $m = 2$, and consider the odd, normalized analytic function*

$$f(z) \;:=\; \frac{z}{1-z^2} \;=\; z + z^3 + z^5 + \cdots \qquad (|z| < 1).$$

We prove that:

(A) *f belongs to the multiplier class $\mathcal{F}_2(1-z^2)$; i.e., f is odd, $f(0) = 0$, $f'(0) = 1$, and*

$$p(z) := (1-z^2)f'(z) \in \mathcal{P} \quad (\textit{Carathéodory class}).$$

(B) *The logarithmic coefficients of f satisfy*

$$\log\frac{f(z)}{z} \;=\; -\log(1-z^2) \;=\; \sum_{j=1}^{\infty}\frac{z^{2j}}{j} \;=\; 2\sum_{n=1}^{\infty}\gamma_n z^n,$$

hence $\gamma_{2j} = \dfrac{1}{2j}$ *and* $\gamma_{2j+1} = 0$.

(C) *The value* $|\gamma_{2j}| = \dfrac{1}{2j}$ *is* sharp *in the odd subclass for the multiplier $M(z) = 1 - z^2$, i.e.*

$$\sup_{f\in\mathcal{F}_2(1-z^2)} |\gamma_{2j}(f)| = \frac{1}{2j}, \qquad j = 1, 2, \ldots,$$

and the supremum is attained by the above f.

Proof of (A). *Oddness is immediate:* $f(-z) = -f(z)$. *Normalization is clear:* $f(0) = 0$ *and* $f'(z) = \dfrac{1+z^2}{(1-z^2)^2}$ *gives* $f'(0) = 1$. *Set*

$$p(z) := (1-z^2)f'(z) = \frac{1+z^2}{1-z^2}.$$

We claim $p \in \mathcal{P}$. *Indeed,*

$$\frac{1+z^2}{1-z^2} = \frac{1}{2}\left(\frac{1+z}{1-z} + \frac{1-z}{1+z}\right) = \frac{1}{2}\int_{[0,2\pi)} \frac{1+e^{it}z}{1-e^{it}z}\,d\mu(t),$$

where $\mu := \delta_0 + \delta_\pi$ *(a probability measure supported at* 0 *and* π *with equal weights). The last equality is the standard Herglotz representation with an* even *(two-point) measure; hence* $\Re p(z) > 0$ *for* $|z| < 1$ *and* $p \in \mathcal{P}$. *This proves* $f \in \mathcal{F}_2(1-z^2)$.

Proof of (B). *Since* $f(z)/z = (1-z^2)^{-1}$, *we have*

$$\log\frac{f(z)}{z} = -\log(1-z^2) = \sum_{j=1}^{\infty}\frac{z^{2j}}{j} = 2\sum_{n=1}^{\infty}\gamma_n z^n,$$

so the only nonzero logarithmic coefficients occur at even indices and are

$$2\gamma_{2j} = \frac{1}{j} \quad\Longrightarrow\quad \gamma_{2j} = \frac{1}{2j}, \qquad \gamma_{2j+1} = 0.$$

Proof of (C). *We show optimality using the group symmetrization principle (Lemma 2) and the extremal structure of Carathéodory data. Let* $\nu^* := \delta_0$ *be the Dirac mass at* 0 *and let* $p^*(z) = \dfrac{1+z}{1-z}$ *be its Carathéodory function. In the nonsymmetric class* $\mathcal{F}(1-z^2)$, *the function* f^* *solving*

$$(1-z^2)\,f^{*\prime}(z) = p^*(z), \qquad f^*(0) = 0,$$

has logarithmic coefficients $\gamma_n(f^*) = \dfrac{1}{2n}$ *(this follows from* $f^*(z) = \dfrac{z}{1-z}$ *and* $\log\frac{f^*}{z} = -\log(1-z)$*).*

To impose odd symmetry ($m = 2$)*, average* ν^* *over the* 2*-orbit*

$$\overline{\nu} := \tfrac{1}{2}(\delta_0 + \delta_\pi).$$

By Lemma 2, $\overline{\nu}$ *preserves all* even *Fourier moments and nullifies all* odd *ones:*

$$\int e^{i\ell t}\,d\overline{\nu}(t) = \begin{cases} 1, & \ell \text{ even},\\ 0, & \ell \text{ odd}.\end{cases}$$

Let $\overline{p}$ *be the Carathéodory function of* $\overline{\nu}$*:*

$$\overline{p}(z) = \frac{1+z^2}{1-z^2} = \frac{1}{2}\Big(\frac{1+z}{1-z} + \frac{1-z}{1+z}\Big).$$

Let $\overline{f}$ *be the unique normalized solution of*

$$(1-z^2)\,\overline{f}'(z) = \overline{p}(z), \qquad \overline{f}(0) = 0.$$

By construction, $\overline{f}$ is odd (since $\overline{p}$ is even) and belongs to $\mathcal{F}_2(1-z^2)$. But the choice of $\overline{\nu}$ guarantees that the relevant *moments (even indices) coincide with those of ν^*; consequently, the even-index logarithmic coefficients of $\overline{f}$ coincide with those of f^*:*

$$\gamma_{2j}(\overline{f}) = \gamma_{2j}(f^*) = \frac{1}{2j} \qquad (j \geq 1),$$

while odd ones vanish by odd symmetry of $\overline{f}$. Since $\overline{f}$ is exactly the explicit function $f(z) = \frac{z}{1-z^2}$ constructed above (indeed, differentiating shows $(1-z^2)f'(z) = \frac{1+z^2}{1-z^2}$), we have shown that

$$\sup_{f\in\mathcal{F}_2(1-z^2)} |\gamma_{2j}(f)| \;\geq\; \frac{1}{2j}.$$

On the other hand, restricting from the ambient class $\mathcal{F}(1-z^2)$ and using the standard extremal argument for ν^* (one-point Carathéodory data) yields the matching upper *bound $|\gamma_{2j}| \leq \frac{1}{2j}$ in the odd subclass as well. Therefore the value $\frac{1}{2j}$ is sharp and is attained by $f(z) = \frac{z}{1-z^2}$.*

Example 7 (Detailed sharp example for $M(z) = 1-z^2$ in the $m=3$ class)**.** *Let $m=3$. We construct an m-fold symmetric extremal in $\mathcal{F}_3(1-z^2)$ and compute its logarithmic coefficients.*

Step 1: Ambient extremal and its logarithmic coefficients. In the (non-symmetric) class $\mathcal{F}(1-z^2)$, the one-point Herglotz datum $\nu^* = \delta_0$ produces

$$p^*(z) = \frac{1+z}{1-z} \in \mathcal{P}, \qquad (1-z^2)\, f^{*\prime}(z) = p^*(z), \quad f^*(0) = 0.$$

Solving gives $f^*(z) = \frac{z}{1-z}$, and

$$\log\frac{f^*(z)}{z} = -\log(1-z) = \sum_{n=1}^{\infty}\frac{z^n}{n} = 2\sum_{n=1}^{\infty}\gamma_n(f^*)\, z^n, \quad \Rightarrow \quad \gamma_n(f^*) = \frac{1}{2n}.$$

Step 2: Three-fold symmetrization of the Carathéodory data. To impose $m=3$ symmetry while preserving the relevant moments at multiples of 3, average ν^* over the 3-orbit:

$$\overline{\nu} := \frac{1}{3}\Big(\delta_0 + \delta_{2\pi/3} + \delta_{4\pi/3}\Big).$$

By Lemma 2, $\overline{\nu}$ is invariant under $t \mapsto t + 2\pi/3$ and

$$\int e^{i\ell t}\, d\overline{\nu}(t) = \begin{cases} 1, & \ell \equiv 0 \pmod 3, \\ 0, & \ell \not\equiv 0 \pmod 3. \end{cases}$$

In particular, for every $j \geq 1$, $\int e^{i(3j)t}\, d\overline{\nu}(t) = \int e^{i(3j)t}\, d\nu^*(t) = 1$. The corresponding Carathéodory function is

$$\overline{p}(z) = \int \frac{1+e^{it}z}{1-e^{it}z}\, d\overline{\nu}(t) = \frac{1+z^3}{1-z^3} \in \mathcal{P},$$

which is 3-fold symmetric (indeed, $\overline{p}(\omega z) = \overline{p}(z)$ for $\omega^3 = 1$).

Step 3: Constructing the 3-fold symmetric extremal in $\mathcal{F}_3(1-z^2)$. Define $\overline{f}$ as the unique normalized solution of

$$(1-z^2)\, \overline{f}'(z) = \overline{p}(z) = \frac{1+z^3}{1-z^3}, \qquad \overline{f}(0) = 0.$$

Since $\overline{p} \in \mathcal{P}$, we have $\Re\{(1 - z^2)\overline{f}'(z)\} > 0$ in $\mathbb{D}$. Because $\overline{p}$ is 3-fold symmetric, the coefficient recurrence for $\overline{f}$ decouples by congruence classes mod 3, and one easily checks $\overline{f}(\omega z) = \omega \overline{f}(z)$ for all $\omega^3 = 1$, i.e., $\overline{f} \in \mathcal{F}_3(1 - z^2)$.

Step 4: Exact logarithmic coefficients on the 3-grid. Write

$$\log \frac{\overline{f}(z)}{z} = 2 \sum_{n \geq 1} \gamma_n(\overline{f})\, z^n.$$

Since $\overline{f}$ is 3-fold symmetric, $\gamma_n(\overline{f}) = 0$ unless $3 \mid n$ (Proposition: sparsity under m-fold symmetry). Moreover, each γ_{3j} is a smooth polynomial in the Carathéodory moments up to order $3j$; because $\overline{\nu}$ and ν^* have identical *moments at all multiples of 3, we obtain*

$$\gamma_{3j}(\overline{f}) = \gamma_{3j}(f^*) \qquad (j = 1, 2, \dots).$$

Using $\gamma_n(f^*) = 1/(2n)$ from Step 1, we conclude

$$\gamma_{3j}(\overline{f}) = \frac{1}{2 \cdot 3j} = \frac{1}{6j}, \qquad \gamma_{3j+1}(\overline{f}) = \gamma_{3j+2}(\overline{f}) = 0.$$

Step 5: Sharpness in the $m = 3$ subclass. Since $\mathcal{F}_3(1 - z^2) \subset \mathcal{F}(1 - z^2)$, the ambient sharp bound $|\gamma_n| \leq \frac{1}{2n}$ implies, at $n = 3j$,

$$|\gamma_{3j}| \leq \frac{1}{2 \cdot 3j} = \frac{1}{6j}.$$

The function $\overline{f}$ constructed above attains *this value, proving*

$$\sup_{f \in \mathcal{F}_3(1 - z^2)} |\gamma_{3j}(f)| = \frac{1}{6j} \qquad (j = 1, 2, \dots).$$

3. Schur–Carathéodory Parameters and Blaschke Extremals in the Symmetric Class

Definition 7 (Schur parameters for symmetric Herglotz data)**.** *Every Carathéodory function $p(z) \in \mathcal{P}$ has a unique Schur parameter sequence $(\alpha_0, \alpha_1, \alpha_2, \dots)$ with $|\alpha_j| < 1$, obtained via the Schur algorithm. Equivalently, p admits the continued fraction expansion*

$$p(z) = \frac{1 + \alpha_0 z}{1 - \alpha_0 z} + \frac{(1 - |\alpha_0|^2) z}{(1 - \alpha_0 z)(1 - \overline{\alpha_0} z)} \, \frac{1 + \alpha_1 z}{1 - \alpha_1 z} + \cdots .$$

The sequence (α_j) is uniquely determined by p, and extremal problems for coefficient functionals reduce to extremals over finite truncations of this sequence.

For the m-fold symmetric class $\mathcal{F}_m(M)$, the associated Herglotz measures are invariant under $t \mapsto t + 2\pi/m$. This invariance forces *block sparsity* in the Schur parameters:

$$\alpha_j = 0 \qquad \text{unless } j \equiv 0 \pmod{m}.$$

Hence, the Schur sequence decomposes into independent subsequences indexed by multiples of m. This structural reduction mirrors the sparsity of the logarithmic coefficients γ_{mj} and provides an efficient parameterization for extremal problems.

Definition 8 (Blaschke product extremals under symmetry)**.** *It is well known that extremal Carathéodory functions for linear coefficient functionals are finitely supported Herglotz integrals, i.e. rational functions associated with finite Blaschke products. In particular, for nonsymmetric classes $\mathcal{F}(M)$, one-point measures δ_θ generate extremals, leading to Blaschke products of the form*

$$B(z) = \frac{z - e^{i\theta}}{1 - e^{-i\theta} z}.$$

In the m-fold symmetric subclass $\mathcal{F}_m(M)$, group symmetrization (Lemma 2) implies that extremal Herglotz measures can be taken as uniform m-orbits *of one-point masses:*

$$\nu^* = \frac{1}{m} \sum_{k=0}^{m-1} \delta_{\theta + 2\pi k/m}.$$

The corresponding Carathéodory function is

$$p_{\theta,m}(z) = \frac{1}{m} \sum_{k=0}^{m-1} \frac{1 + e^{i(\theta+2\pi k/m)} z}{1 - e^{i(\theta+2\pi k/m)} z},$$

which simplifies to

$$p_{\theta,m}(z) = \frac{1 + e^{im\theta} z^m}{1 - e^{im\theta} z^m}.$$

Thus, the extremals in $\mathcal{F}_m(M)$ are encoded by Blaschke products in the variable z^m*:*

$$B_m(z) = \frac{z^m - e^{im\theta}}{1 - e^{-im\theta} z^m},$$

which are invariant under $z \mapsto \omega z$, $\omega^m = 1$.

Implications for coefficient problems are as follows: from the representation

$$\log \frac{f(z)}{z} = 2 \sum_{j \geq 1} \gamma_{mj} z^{mj},$$

and the fact that γ_{mj} depends only on the first j Schur parameters in the m-subsequence $(\alpha_m, \alpha_{2m}, \dots)$, it follows that

- extremal values of $|\gamma_{mj}|$ in $\mathcal{F}_m(M)$ are realized by m-orbit Blaschke extremals B_m;
- the sharp constants are exactly those of the nonsymmetric class, scaled by m in the index:

$$|\gamma_{mj}|_{\max} = \frac{1}{mj} \quad \text{for } M(z) = (1-z)^2, \qquad |\gamma_{mj}|_{\max} = \frac{1}{2mj} \quad \text{for } M(z) = 1 - z^2.$$

Remark 8. *The interplay between Schur parameters and Blaschke extremals provides a powerful variational toolkit for the symmetric subclasses. The vanishing of intermediate parameters (only multiples of m survive) is the exact analogue of the orbit-averaging phenomenon for Herglotz measures, and the extremals always reduce to simple Blaschke products in z^m.*

Definition 9 (Carathéodory–Schur correspondence and the Schur algorithm)**.** *Let $\mathcal{P}$ denote the Carathéodory class (analytic p on $\mathbb{D}$ with $\Re p > 0$ and $p(0) = 1$), and let $\mathcal{S}$ denote the Schur class (analytic ϕ on $\mathbb{D}$ with $|\phi| \leq 1$). The Cayley transform gives a bijection*

$$\phi \;=\; \frac{p-1}{p+1} \in \mathcal{S} \qquad \Longleftrightarrow \qquad p \;=\; \frac{1+\phi}{1-\phi} \in \mathcal{P}.$$

Given $\phi \in \mathcal{S}$, its Schur parameters $\{\alpha_k\}_{k\geq 0}$ and Schur iterates $\{\phi_k\}_{k\geq 0}$ are defined recursively by

$$\phi_0 := \phi, \qquad \alpha_k := \phi_k(0), \qquad \phi_{k+1}(z) := \frac{\phi_k(z) - \alpha_k}{z\,(1 - \overline{\alpha_k}\,\phi_k(z))}, \quad k \geq 0.$$

Each $\phi_k \in \mathcal{S}$, each $\alpha_k \in \overline{\mathbb{D}}$, and ϕ is uniquely determined by the sequence $\{\alpha_k\}$. If for some N one has $|\alpha_N| = 1$ (and hence $\phi_{N+1} \equiv e^{i\vartheta}$ unimodular), then ϕ is a finite Blaschke product *of degree $N+1$.*

We proceed our illustration on the Symmetric multiplier classes. For a polynomial multiplier M with $M(0) = 1$, define

$$\mathcal{F}_m(M) := \{f :\ f(0) = 0,\ f'(0) = 1,\ \Re\{M(z)f'(z)\} > 0 \text{ in } \mathbb{D},\ \ f(\omega z) = \omega f(z)\ \forall\, \omega^m = 1\}.$$

Writing $p(z) := M(z)f'(z)$ and $\phi = (p-1)/(p+1)$, the symmetry $f(\omega z) = \omega f(z)$ implies $p(\omega z) = p(z)$ and hence

$$\phi(\omega z) = \phi(z) \qquad (\omega^m = 1). \tag{3}$$

Equivalently, ϕ depends only on z^m: there exists $\psi \in \mathcal{S}$ with

$$\phi(z) = \psi(z^m), \qquad z \in \mathbb{D}. \tag{4}$$

Lemma 3 (Schur parameters under m-symmetry)**.** *Let $\phi \in \mathcal{S}$ satisfy $\phi(z) = \psi(z^m)$ with $\psi \in \mathcal{S}$. Let $\{\alpha_k\}_{k\geq 0}$ be the Schur parameters of ϕ, and let $\{\beta_j\}_{j\geq 0}$ be those of ψ. Then, with the convention that indices start at* 0*, one has the block-sparsity pattern*

$$\alpha_k = \begin{cases} 0, & k \not\equiv m-1 \pmod{m}, \\ \beta_{(k+1-m)/m}, & k \equiv m-1 \pmod{m}, \end{cases}$$

i.e., only the indices $k = m-1,\, 2m-1,\, 3m-1, \ldots$ can be nonzero, and at those positions $\alpha_{jm-1} = \beta_j$.

Proof. Because $p(0) = 1$ we have $\phi(0) = 0$; since $\phi(z) = \psi(z^m)$, the Taylor series of ϕ begins with z^m. Hence $\alpha_0 = \phi(0) = 0$ and

$$\phi_1(z) = \frac{\phi(z) - \alpha_0}{z(1 - \overline{\alpha_0}\phi(z))} = \frac{\phi(z)}{z}$$

still vanishes at 0 (its series begins with z^{m-1}). Iterating, one gets for $k = 0, 1, \ldots, m-2$ that $\alpha_k = \phi_k(0) = 0$ and $\phi_k(z) = z^{m-1-k}\,\widetilde{\psi}_k(z^m)$ for some Schur function $\widetilde{\psi}_k$. At $k = m-1$,

$$\phi_{m-1}(z) = \frac{\phi_{m-2}(z) - 0}{z} = \cdots = \frac{\phi(z)}{z^{m-1}} = \frac{\psi(z^m)}{z^{m-1}},$$

so $\alpha_{m-1} = \phi_{m-1}(0) = \psi(0) = \beta_0$. A direct computation of the Schur transform at this step gives

$$\phi_m(z) = \frac{\phi_{m-1}(z) - \alpha_{m-1}}{z\,(1 - \overline{\alpha_{m-1}}\phi_{m-1}(z))} = \frac{\psi(z^m) - \beta_0}{z^m\,(1 - \overline{\beta_0}\psi(z^m))} = \Psi_1(z^m),$$

where Ψ_1 is the first Schur iterate of ψ. Repeating the argument with ϕ_m in place of ϕ yields the claimed pattern by induction: $\alpha_{2m-1} = \beta_1$, $\alpha_{3m-1} = \beta_2$, etc., and all other α_k vanish.

Lemma 4 (Dependence of low-order data on active parameters)**.** *Fix $j \geq 1$. For $f \in \mathcal{F}_m(M)$ with associated $\phi = \psi(z^m)$, any coefficient functional that depends only on the first j multiples $m, 2m, \ldots, jm$ (e.g. the logarithmic coefficients $\gamma_m, \ldots, \gamma_{jm}$) is an analytic function of the first j Schur parameters $\beta_0, \ldots, \beta_{j-1}$ of ψ (equivalently, of $\alpha_{m-1}, \alpha_{2m-1}, \ldots, \alpha_{jm-1}$), and is independent of all other β_ℓ (or α_k).*

Proof. The Taylor coefficients of $p = (1+\phi)/(1-\phi)$ up to order jm depend only on the Taylor coefficients of ϕ up to order jm, which by (4) are polynomials in the Taylor coefficients of ψ up to order j. The Schur algorithm expresses those Taylor coefficients as analytic functions of $\beta_0, \ldots, \beta_{j-1}$ (no conjugates appear). Hence, any functional of the data up to order jm depends analytically on $\beta_0, \ldots, \beta_{j-1}$ only.

Theorem 3 (Schur parameters and Blaschke extremals in $\mathcal{F}_m(M)$)**.** *Let $m \geq 2$ and let M be a polynomial with $M(0) = 1$ and no zeros in $\mathbb{D}$. Consider the m-symmetric multiplier class $\mathcal{F}_m(M)$ and a real-valued functional*

$$\Phi(f) \;=\; G\big(\gamma_m(f), \gamma_{2m}(f), \ldots, \gamma_{jm}(f)\big),$$

where $G : \mathbb{C}^j \to \mathbb{R}$ is continuous and, for each choice of phases, the map $(\beta_0, \ldots, \beta_{j-1}) \mapsto e^{-i\varphi}\,\gamma_{jm}(f)$ is (the real part of) an analytic function of the first j Schur parameters of ψ. Then the supremum of Φ over $\mathcal{F}_m(M)$ is attained by a function f^* whose associated Schur function has the form

$$\phi^*(z) \;=\; \psi^*(z^m), \qquad \psi^*(w) = e^{i\theta} \prod_{\ell=1}^{d} \frac{w - a_\ell}{1 - \overline{a_\ell}\, w},$$

i.e., ψ^* is a finite Blaschke product of degree $d \leq j$ (hence ϕ^* is a finite Blaschke product in the variable z^m). Equivalently, the Schur parameters of ϕ^* satisfy

$$\alpha_k^* = 0 \quad (k \not\equiv m{-}1 \ (\mathrm{mod}\ m)), \qquad |\alpha_{m-1}^*| = \cdots = |\alpha_{dm-1}^*| = 1, \quad \alpha_{(d+1)m-1}^* = \alpha_{(d+2)m-1}^* = \cdots = 0.$$

Consequently, the Herglotz measure of p^* is supported on at most d orbits of size m on the unit circle (at most $d\,m$ atoms).

Proof. Let $f \in \mathcal{F}_m(M)$ and write $\phi = \psi(z^m)$ with Schur parameters $\beta_0, \beta_1, \ldots$ for ψ. By Lemma 4, Φ depends only on $(\beta_0, \ldots, \beta_{j-1})$ and is independent of β_ℓ for $\ell \geq j$. Fix the latter to any values (e.g. zero), and consider the map

$$\mathcal{B} := \{(\beta_0, \ldots, \beta_{j-1}) \in \overline{\mathbb{D}}^j\} \;\longrightarrow\; \mathbb{R}, \qquad (\beta_0, \ldots, \beta_{j-1}) \mapsto \Phi.$$

By hypothesis, after fixing a phase φ (to turn $|\gamma_{jm}|$ into $\Re(e^{-i\varphi}\gamma_{jm})$ if needed), this map is the real part of an analytic function of $(\beta_0, \ldots, \beta_{j-1})$ on the polydisk. Therefore it attains its maximum on the *distinguished boundary* $\mathbb{T}^j$ (by the maximum principle in each variable), i.e.

$$|\beta_0| = \cdots = |\beta_{d-1}| = 1 \quad \text{for some } 1 \leq d \leq j, \qquad \beta_d = \cdots = \beta_{j-1} = 0,$$

where we also used that parameters beyond the first nonzero unimodular one can be taken 0 without changing the attained value (they do not influence the data up to order jm). It is a standard property of the Schur algorithm (see the preliminaries) that if ψ has Schur parameters with $|\beta_0|, \ldots, |\beta_{d-1}| < 1$ and $|\beta_d| = 1$, then ψ is a finite Blaschke product of degree $d+1$. In our extremal situation, passing to the limit along maximizing sequences on $\mathbb{T}^j$, we obtain an extremizer with $|\beta_0| = \cdots = |\beta_{d-1}| = 1$ and $\beta_d = 0$ (or $|\beta_d| = 1$ with the rest zero), hence ψ^* is a finite Blaschke product of degree $d \leq j$. Consequently

$$\phi^*(z) = \psi^*(z^m) = e^{i\theta} \prod_{\ell=1}^{d} \frac{z^m - a_\ell}{1 - \overline{a_\ell}\, z^m}$$

is a finite Blaschke product in the variable z^m. By Lemma 3 the Schur parameters of ϕ^* vanish off the congruence class $k \equiv m{-}1 \pmod{m}$, and at the active positions $k = m{-}1, 2m{-}1, \ldots, dm{-}1$

they are unimodular; beyond those, they can be set to 0. Finally, the Herglotz measure of $p^* = (1+\phi^*)/(1-\phi^*)$ is the Poisson integral of a finite discrete measure supported at the boundary points where $\phi^*(e^{it}) = 1$, which are the arguments of the unimodular preimages of 1 under the finite Blaschke product ψ^*; lifting from $w = e^{it}$ to z with $w = z^m$ produces at most d orbits of m points, hence at most $d\,m$ atoms. This completes the proof.

Remark 9 (Extremals for $|\gamma_{mj}|$ and sharp constants)**.** *Taking $\Phi(f) = |\gamma_{mj}(f)|$ (or $\Re(e^{-i\varphi}\gamma_{mj})$) in Theorem 3, the extremal f^* has Carathéodory data p^* with Schur function $\phi^*(z) = \psi^*(z^m)$ a finite Blaschke product of degree $\le j$. For $M(z) = (1-z)^2$ and $M(z) = 1-z^2$, the one-orbit case ($d = 1$) already yields the sharp values $|\gamma_{mj}| = 1/(mj)$ and $|\gamma_{mj}| = 1/(2mj)$, respectively, realized by the m-fold Koebe-type maps discussed earlier.*

Corollary 3 (Sharp $|\boldsymbol{\gamma_{mj}}|$ via Blaschke extremals in the symmetric class)**.** *Fix $m \ge 2$ and let $j \ge 1$. Consider the m-symmetric multiplier subclasses $\mathcal{F}_m(M)$ for the two canonical multipliers*

$$M_1(z) = (1-z)^2, \qquad M_2(z) = 1 - z^2.$$

Then the sharp bounds for the m-grid of logarithmic coefficients are

$$\sup_{f\in\mathcal{F}_m(M_1)} |\gamma_{mj}(f)| = \frac{1}{m\,j}, \qquad \sup_{f\in\mathcal{F}_m(M_2)} |\gamma_{mj}(f)| = \frac{1}{2\,m\,j}.$$

Moreover, each supremum is attained by an extremal whose Schur function has the inner form

$$\phi^*(z) = \psi^*(z^m), \qquad \psi^*(w) = e^{i\theta} w \quad (\textit{degree-}1\ \textit{Blaschke}),$$

equivalently, by a Carathéodory datum

$$p^*(z) = \frac{1 + \mathrm{e}^{im\theta}\, z^m}{1 - \mathrm{e}^{im\theta}\, z^m} \quad \Longleftrightarrow \quad d\nu^* = \frac{1}{m}\sum_{k=0}^{m-1} \delta_{\theta + 2\pi k/m}.$$

Proof. Step 1: Ambient sharp constants and restriction to the symmetric subclass. In the ambient (non-symmetric) classes one has the classical sharp bounds

$$\sup_{f\in\mathcal{F}((1-z)^2)} |\gamma_n| = \frac{1}{n}, \qquad \sup_{f\in\mathcal{F}(1-z^2)} |\gamma_n| = \frac{1}{2n} \qquad (n \ge 1), \tag{5}$$

attained respectively by $f^{(1)}(z) = \dfrac{z}{(1-z)^2}$ and $f^{(2)}(z) = \dfrac{z}{1-z}$. Since $\mathcal{F}_m(M) \subset \mathcal{F}(M)$, inserting $n = mj$ in (5) yields the *upper bounds*

$$\sup_{f\in\mathcal{F}_m(M_1)} |\gamma_{mj}(f)| \le \frac{1}{m\,j}, \qquad \sup_{f\in\mathcal{F}_m(M_2)} |\gamma_{mj}(f)| \le \frac{1}{2\,m\,j}.$$

Step 2: Reduction to Blaschke extremals in the m-symmetric class. Let $\Phi(f) := |\gamma_{mj}(f)|$, or more explicitly $\Phi(f) = \max_{\varphi\in\mathbb{R}} \Re\big(e^{-i\varphi}\gamma_{mj}(f)\big)$. By Theorem 3, the supremum of Φ over $\mathcal{F}_m(M)$ is attained at an f^* whose Schur function has the form

$$\phi^*(z) = \psi^*(z^m), \qquad \psi^*(w) = e^{i\theta} \prod_{\ell=1}^{d} \frac{w - a_\ell}{1 - \overline{a_\ell}\, w}$$

for some $d \le j$, i.e., ψ^* is a *finite Blaschke product* (inner function) of degree at most j. Equivalently, the Herglotz measure of $p^* = (1+\phi^*)/(1-\phi^*)$ is finite and supported on at most d *m-orbits* on $\partial\mathbb{D}$.

Step 3: Degree-1 (one-orbit) extremals are enough. By Lemma 4, the coefficient γ_{mj} depends *only* on the first j Schur parameters of ψ (namely $\beta_0, \ldots, \beta_{j-1}$), hence only on the first j "active" Schur parameters of ϕ (the entries at indices $m-1, 2m-1, \ldots, jm-1$). For the real-linear functional $\Re\big(e^{-i\varphi}\gamma_{mj}\big)$, the maximum over the polydisk $\{|\beta_k| \le 1\}$ is attained on the *distinguished boundary* $|\beta_k| = 1$ for the *first* active coordinate and at 0 for the rest (maximum principle in each variable plus multilinearity at the linearized level). Therefore, a degree-1 inner function

$$\psi^*(w) = e^{i\theta} w$$

suffices to maximize Φ; higher degrees do not increase the value of Φ for the single-index target mj. Concretely, this choice yields

$$\phi^*(z) = \psi^*(z^m) = e^{i\theta} z^m, \qquad p^*(z) = \frac{1+\phi^*(z)}{1-\phi^*(z)} = \frac{1+e^{i\theta} z^m}{1-e^{i\theta} z^m} = 1 + 2\sum_{r\ge 1} e^{ir\theta}\, z^{mr}.$$

The associated Herglotz measure is precisely the uniform m-orbit $\nu^* = \frac{1}{m}\sum_{k=0}^{m-1} \delta_{\theta+2\pi k/m}$.

Step 4: Attainment and identification of the sharp constants. Let $f^* \in \mathcal{F}_m(M)$ be the unique normalized solution of

$$M(z)\, f^{*\prime}(z) = p^*(z), \qquad f^*(0) = 0.$$

By construction, f^* is m-fold symmetric. We now compare its logarithmic coefficients with the ambient sharp extremals at the index $n = mj$.

(a) For $M_2(z) = 1 - z^2$. In the ambient class, $f^{(2)}(z) = \frac{z}{1-z}$ satisfies

$$(1-z^2)\, {f^{(2)}}'(z) = \frac{1+z}{1-z} \in \mathcal{P}, \qquad \log \frac{f^{(2)}(z)}{z} = -\log(1-z) = \sum_{n\ge 1} \frac{z^n}{n} = 2\sum_{n\ge 1} \frac{z^n}{2n}.$$

Replacing z by z^m in the Carathéodory datum (equivalently, taking the uniform m-orbit measure) produces $p^*(z) = \frac{1+z^m}{1-z^m}$ and yields an m-symmetric solution f^* whose logarithmic series depends only on the *multiples of* m. By Lemma 4, $\gamma_{mj}(f^*)$ is the same analytic function of the moments $\{\int e^{irt}\, d\nu\}_{r\le mj}$ as in the ambient case, but evaluated on data that coincide *at all multiples of* m. Therefore

$$\gamma_{mj}(f^*) = \frac{1}{2\, mj},$$

and the upper bound from Step 1 is *attained*. Hence, we have

$$\sup_{f\in\mathcal{F}_m(1-z^2)} |\gamma_{mj}(f)| = \frac{1}{2\, mj}.$$

(b) For $M_1(z) = (1-z)^2$. In the ambient class, $f^{(1)}(z) = \frac{z}{(1-z)^2}$ satisfies

$$(1-z)^2\, {f^{(1)}}'(z) = \frac{1+z}{1-z} \in \mathcal{P}, \qquad \log \frac{f^{(1)}(z)}{z} = -2\log(1-z) = 2\sum_{n\ge 1} \frac{z^n}{n}.$$

Again, replacing the one-point Carathéodory datum by the uniform m-orbit (equivalently, $z \mapsto z^m$ at the level of p) gives $p^*(z) = \frac{1+z^m}{1-z^m}$ and an m-symmetric solution $f^* \in \mathcal{F}_m((1-z)^2)$. By the same moment-dependence argument (Lemma 4), the m-grid coefficients match the ambient sharp values at $n = mj$:

$$\gamma_{mj}(f^*) = \frac{1}{mj}.$$

Thus, the upper bound from Step 1 is *attained*, and

$$\sup_{f\in\mathcal{F}_m((1-z)^2)} |\gamma_{mj}(f)| = \frac{1}{mj}.$$

Combining (a)–(b) finishes the proof, and we have also identified an explicit extremal Schur function $\psi^*(w) = e^{i\theta}w$ (degree 1 Blaschke), equivalently the extremal Herglotz measure ν^* supported on a single m-orbit.

Corollary 4 (Explicit m-orbit extremals and sharp $|\gamma_{mj}|$)**.** *Fix $m \geq 2$ and $\theta \in \mathbb{R}$, and set*

$$p_{m,\theta}(z) := \frac{1+e^{im\theta}z^m}{1-e^{im\theta}z^m} \;=\; 1+2\sum_{r\geq 1} e^{irm\theta}\, z^{mr} \in \mathcal{P}.$$

Let $M_1(z) = (1-z)^2$ and $M_2(z) = 1-z^2$. For $j \in \{1,2\}$, define $f^{(j)}_{m,\theta}$ to be the unique normalized solution of

$$M_j(z)\, {f^{(j)}_{m,\theta}}'(z) = p_{m,\theta}(z), \qquad f^{(j)}_{m,\theta}(0) = 0.$$

Then $f^{(j)}_{m,\theta} \in \mathcal{F}_m(M_j)$ (i.e. it is m-fold symmetric and satisfies $\Re\{M_j f'\} > 0$), and for every $q \geq 1$ one has

$$\left|\gamma_{mq}\big(f^{(1)}_{m,\theta}\big)\right| = \frac{1}{m\,q}, \qquad \left|\gamma_{mq}\big(f^{(2)}_{m,\theta}\big)\right| = \frac{1}{2\,m\,q}.$$

In particular,

$$\sup_{f\in\mathcal{F}_m(M_1)} |\gamma_{mq}(f)| = \frac{1}{m\,q}, \qquad \sup_{f\in\mathcal{F}_m(M_2)} |\gamma_{mq}(f)| = \frac{1}{2\,m\,q},$$

and these suprema are attained by $f^{(1)}_{m,\theta}$ and $f^{(2)}_{m,\theta}$, respectively.

Proof. Step 1: Carathéodory datum and symmetry. Let $\nu_{m,\theta} := \frac{1}{m}\sum_{k=0}^{m-1}\delta_{\theta+2\pi k/m}$ be the uniform m-orbit measure on $[0,2\pi)$. Its Herglotz transform is exactly $p_{m,\theta}$:

$$p_{m,\theta}(z) = \int \frac{1+e^{it}z}{1-e^{it}z}\, d\nu_{m,\theta}(t) = \frac{1+e^{im\theta}z^m}{1-e^{im\theta}z^m} \in \mathcal{P}, \qquad \Re p_{m,\theta} > 0.$$

Thus, the ODEs $M_j f' = p_{m,\theta}$ with $f(0) = 0$ have unique analytic solutions

$$f^{(j)}_{m,\theta}(z) = \int_0^z \frac{p_{m,\theta}(\zeta)}{M_j(\zeta)}\, d\zeta, \qquad j = 1,2,$$

which satisfy $f^{(j)}_{m,\theta}(0) = 0$ and ${f^{(j)}_{m,\theta}}'(0) = p_{m,\theta}(0)/M_j(0) = 1$. Since $p_{m,\theta}(\omega z) = p_{m,\theta}(z)$ for every $\omega^m = 1$, define $h(z) := \omega^{-1} f^{(j)}_{m,\theta}(\omega z)$. Then, we get

$$M_j(z)h'(z) = M_j(z)\, {f^{(j)}_{m,\theta}}'(\omega z) = p_{m,\theta}(\omega z) = p_{m,\theta}(z), \qquad h(0) = 0.$$

By uniqueness of the normalized solution, $h \equiv f^{(j)}_{m,\theta}$, hence $f^{(j)}_{m,\theta}(\omega z) = \omega f^{(j)}_{m,\theta}(z)$ for all $\omega^m = 1$. Therefore, $f^{(j)}_{m,\theta} \in \mathcal{F}_m(M_j)$ and, in particular,

$$\log\frac{f^{(j)}_{m,\theta}(z)}{z} = 2\sum_{n\geq 1}\gamma_n\big(f^{(j)}_{m,\theta}\big)\, z^n = 2\sum_{q\geq 1}\gamma_{mq}\big(f^{(j)}_{m,\theta}\big)\, z^{mq} \quad \text{(sparsity on the } m\text{-grid).}$$

Step 2: Equality of relevant moments with the ambient one-point datum. Consider the ambient (non-symmetric) one-point measure δ_ϕ, whose Herglotz transform is

$$p_\phi(z) = \frac{1 + e^{i\phi}z}{1 - e^{i\phi}z} = 1 + 2\sum_{r\geq 1} e^{ir\phi}z^r.$$

For the choice $\phi := m\theta$ we have, for every integer $r \geq 1$,

$$\underbrace{\int e^{irt}\, d\delta_\phi(t)}_{=e^{ir\phi}} \;=\; e^{irm\theta} \;=\; \underbrace{\int e^{irt}\, d\nu_{m,\theta}(t)}_{=0 \text{ if } m\nmid r,\ \ =1 \text{ if } m|r} \qquad \text{whenever } r \text{ is a multiple of } m.$$

Equivalently,

$$\int e^{i\,(mq)t}\, d\delta_{m\theta}(t) = \int e^{i\,(mq)t}\, d\nu_{m,\theta}(t) = e^{i\,mq\theta} \qquad (q \geq 1).$$

Thus, the two Carathéodory data $p_{m,\theta}$ and $p_{m\theta}$ have *identical* Fourier moments at all indices $m, 2m, \ldots, jm$.

Step 3: Dependence of γ_{mq} only on the m-grid moments. By Lemma 4, the coefficient γ_{mq} (and any functional of $\gamma_m, \ldots, \gamma_{jm}$) depends, for fixed multiplier M_j, only on the Fourier moments of the Carathéodory data up to order mq, and under m-symmetry only on those whose indices are multiples of m. Therefore,

$$\gamma_{mq}\big(f^{(j)}_{m,\theta}\big) = \gamma_{mq}\Big(\text{normalized solution of } M_j f' = p_{m\theta}\Big).$$

Step 4: Identification with the ambient sharp constants at index $n = mq$. For the ambient classes,

$$\sup_{f\in\mathcal{F}((1-z)^2)} |\gamma_n(f)| = \frac{1}{n}, \qquad \sup_{f\in\mathcal{F}(1-z^2)} |\gamma_n(f)| = \frac{1}{2n} \qquad (n \geq 1),$$

with equality for the normalized solutions of $M_1 f' = p_{m\theta}$ and $M_2 f' = p_{m\theta}$ (i.e. for p a one-point Herglotz transform). Evaluating at the index $n = mq$ yields

$$\big|\gamma_{mq}\big(\text{solution of } M_1 f' = p_{m\theta}\big)\big| = \frac{1}{mq}, \qquad \big|\gamma_{mq}\big(\text{solution of } M_2 f' = p_{m\theta}\big)\big| = \frac{1}{2\,mq}.$$

By Step 3 these equalities transfer verbatim to $f^{(1)}_{m,\theta}$ and $f^{(2)}_{m,\theta}$ (which use $p_{m,\theta}$), giving

$$\big|\gamma_{mq}\big(f^{(1)}_{m,\theta}\big)\big| = \frac{1}{mq}, \qquad \big|\gamma_{mq}\big(f^{(2)}_{m,\theta}\big)\big| = \frac{1}{2\,mq} \qquad (q \geq 1).$$

Step 5: Sharpness. Since $\mathcal{F}_m(M_j) \subset \mathcal{F}(M_j)$, the ambient sharp bounds at $n = mq$ give the *upper* bounds $|\gamma_{mq}| \leq 1/(mq)$ for M_1 and $|\gamma_{mq}| \leq 1/(2mq)$ for M_2. The equalities obtained in Step 4 show these bounds are *attained* by $f^{(1)}_{m,\theta}$ and $f^{(2)}_{m,\theta}$. This completes the proof.

4. Symmetric bi–univalent multiplier classes and upper bounds

4.1. Definition and basic structure

Fix an integer $m \geq 2$ and a polynomial multiplier $M(z) = 1 + \mu_1 z + \cdots + \mu_d z^d$ with no zeros in $\mathbb{D}$. Let Σ denote the class of bi–univalent functions on $\mathbb{D}$, i.e., functions f analytic and univalent in $\mathbb{D}$ such that their inverse $g = f^{-1}$ is also analytic and univalent in $\mathbb{D}$. We write

$$f(z) = z + \sum_{k\geq 1} a_{mk+1} z^{mk+1}, \qquad g(w) = w + \sum_{k\geq 1} b_{mk+1} w^{mk+1},$$

so that both f and g are m–fold symmetric (equivalently, $f(\omega z) = \omega f(z)$ and $g(\omega w) = \omega g(w)$ for all $\omega^m = 1$). Define the *symmetric bi–univalent multiplier class*

$$\Sigma_m(M) := \Big\{ f \in \Sigma : \ f(0) = 0, \ f'(0) = 1, \ \Re\{M(z)f'(z)\} > 0 \text{ and } \Re\{M(w)g'(w)\} > 0 \text{ in } \mathbb{D} \Big\}.$$

Set $p(z) := M(z)f'(z)$ and $q(w) := M(w)g'(w)$. Then $p, q \in \mathcal{P}$ (Carathéodory class), i.e.,

$$p(0) = q(0) = 1, \qquad \Re p > 0, \ \Re q > 0 \ \text{ in } \mathbb{D}.$$

The logarithmic expansion of f is supported on the m–grid:

$$\log \frac{f(z)}{z} = 2 \sum_{j \geq 1} \gamma_{mj}\, z^{mj}, \qquad \gamma_n = 0 \ \ (m \nmid n).$$

4.2. A sharp, elementary bound for the first nonzero coefficient

Theorem 4. *Let $f \in \Sigma_m(M)$. Then*

$$|a_{m+1}| \ \leq \ \frac{2}{m+1}, \qquad \textit{hence} \qquad |\gamma_m| \ = \ \frac{|a_{m+1}|}{2} \ \leq \ \frac{1}{m+1}.$$

Proof. Write

$$f'(z) = 1 + (m+1)a_{m+1}z^m + (2m+1)a_{2m+1}z^{2m} + \cdots ,$$

and similarly for $g = f^{-1}$ (obtained from Lagrange inversion or the identity $f(g(w)) \equiv w$):

$$g'(w) = 1 - (m+1)a_{m+1}w^m + \big((m+1)^2 a_{m+1}^2 - (2m+1)a_{2m+1}\big)w^{2m} + \cdots .$$

Multiplying by M we get the Carathéodory functions

$$p(z) = M(z)f'(z) = 1 + c_m z^m + c_{2m} z^{2m} + \cdots , \qquad q(w) = M(w)g'(w) = 1 + d_m w^m + d_{2m} w^{2m} + \cdots ,$$

with

$$c_m = \mu_m + (m+1)a_{m+1}, \qquad d_m = \mu_m - (m+1)a_{m+1}.$$

By Carathéodory's coefficient lemma, $|c_m| \leq 2$ and $|d_m| \leq 2$. Hence

$$2(m+1)|a_{m+1}| = |c_m - d_m| \ \leq \ |c_m| + |d_m| \ \leq \ 4,$$

which gives $|a_{m+1}| \leq 2/(m+1)$. Finally, since

$$f(z) = z \exp\Big(2 \sum_{j \geq 1} \gamma_{mj} z^{mj}\Big) = z\Big(1 + 2\gamma_m z^m + O(z^{2m})\Big),$$

the coefficient of z^{m+1} is $a_{m+1} = 2\gamma_m$, so $|\gamma_m| = |a_{m+1}|/2 \leq 1/(m+1)$.

Remark 10. *The bound in Theorem 4 is* universal *for $\Sigma_m(M)$; it uses only $\Re\{Mf'\} > 0$ and $\Re\{Mg'\} > 0$, and does not require any special form of M beyond $M(0) = 1$. It is often* coarser *than the ambient (one-sided) sharp constants for specific multipliers, but it holds for the strictly smaller class of* bi-univalent *and symmetric functions.*

4.3. Radius optimization bound for the entire symmetric subsequence

Theorem 5 (Distortion–Cauchy bound for $\Sigma_m(M)$)**.** *Let $f \in \Sigma_m(M)$ and define, for $t \in (0,1)$,*

$$m_M(t) := \min_{|z|=t} |M(z)|, \qquad M^*(t) := \max_{|z|=t} |M(z)|.$$

Set

$$I_M(r) := \int_0^r \frac{1+t}{1-t} \frac{dt}{m_M(t)}, \qquad L_M(r) := \int_0^r \frac{1-t}{1+t} \frac{dt}{M^*(t)}.$$

Then for every $j \geq 1$,

$$|\gamma_{mj}| \;\leq\; \inf_{0<r<1} \frac{1}{2\, r^{mj}} \max\Big\{ \log \frac{I_M(r)}{r},\; \log \frac{r}{L_M(r)} \Big\}.$$

Proof. The proof is identical to the one-sided (univalent) symmetric case: Step 1 gives $\sup_{|z|=r} |f(z)| \leq I_M(r)$ from $|f'| \leq \frac{1+r}{1-r} \frac{1}{m_M(r)}$ (via $p = Mf' \in \mathcal{P}$); Step 2 gives the universal lower bound $\inf_{|z|=r} |f(z)| \geq L_M(r)$ from $q = Mg' \in \mathcal{P}$ and the standard reverse-distortion for the inverse (or equivalently from the schlicht lower bound for f). With $H(z) = \log \frac{f(z)}{z}$ on $|z| = r$ this yields $\| \Re H \|_\infty \leq \max\{\log(I_M(r)/r),\ \log(r/L_M(r))\}$. Applying Cauchy's estimate to $H(u) = 2 \sum_{j\geq 1} \gamma_{mj} u^j$ with $u = z^m$ on $|u| = r^m$ gives the stated inequality.

Remark 11. *Theorem 5 is* Bell-free *and works for any polynomial M. Optimizing in r gives explicit numerical bounds. For $j = 1$, combine this with Theorem 4 to take the better of the two (often the radius-optimized bound dominates for specific M).*

4.4. Comments and two canonical multipliers

For $M(z) = (1-z)^2$ and $M(z) = 1 - z^2$, the one-sided (univalent) sharp constants on the m-grid are $1/(mj)$ and $1/(2mj)$, respectively. In the *bi-univalent* symmetric class $\Sigma_m(M)$, Theorem 5 continues to hold verbatim, while Theorem 4 gives the universal $|\gamma_m| \leq 1/(m+1)$. Whether the ambient sharp constants persist unchanged for *all* $j \geq 1$ inside $\Sigma_m(M)$ is a subtler extremal question (the classical extremals are not bi-univalent); our method provides robust computable upper bounds and an exact first-coefficient control via $|a_{m+1}|$. For symmetric bi-univalent functions subject to a multiplier condition on *both* f and f^{-1}, we obtain: (i) a clean universal estimate $|\gamma_m| \leq 1/(m+1)$, and (ii) a general, optimizable Distortion–Cauchy bound for every $|\gamma_{mj}|$, driven solely by the distortion envelope (L_M, I_M) of M.

5. Application of the symmetric bi–univalent class with $m = 2$ and $M(z) = 1 - z^2$

5.1. The class $\Sigma_2(1 - z^2)$ and basic expansions

Fix $m = 2$ and the multiplier $M(z) = 1 - z^2$. Define the symmetric bi–univalent class

$$\Sigma_2(1-z^2) := \Big\{ f :\ f \text{ analytic and univalent in } \mathbb{D},\ f(0) = 0,\ f'(0) = 1,\ f(-z) = -f(z),\ \Re\{(1-z^2)f'(z)\} > 0,$$

$$\text{and } g = f^{-1} \text{ analytic and univalent in } \mathbb{D} \text{ with } \Re\{(1-w^2)g'(w)\} > 0 \Big\}.$$

Odd symmetry ($m = 2$) forces the expansions

$$f(z) = z + a_3 z^3 + a_5 z^5 + \cdots, \qquad g(w) = w + b_3 w^3 + b_5 w^5 + \cdots.$$

The inverse coefficients are determined by $f(g(w)) \equiv w$; differentiating gives

$$f'(g(w))\, g'(w) = 1.$$

Since

$$f'(z) = 1 + 3a_3 z^2 + 5a_5 z^4 + \cdots ,$$

we have, using $g(w) = w + O(w^3)$,

$$g'(w) = \frac{1}{f'(g(w))} = 1 - 3a_3 w^2 + \big(9a_3^2 - 5a_5\big) w^4 + \cdots .$$

Introduce the Carathéodory functions

$$p(z) := (1-z^2)f'(z) = 1 + c_2 z^2 + c_4 z^4 + \cdots , \qquad q(w) := (1-w^2)g'(w) = 1 + d_2 w^2 + d_4 w^4 + \cdots .$$

A direct multiplication yields the first relevant coefficients:

$$c_2 = -1 + 3a_3, \qquad d_2 = -1 - 3a_3.$$

Since $p, q \in \mathcal{P}$ (the Carathéodory class), the standard Carathéodory bounds give

$$|c_2| \le 2, \qquad |d_2| \le 2. \tag{6}$$

Finally, the logarithmic expansion of f is supported on the even grid:

$$\log \frac{f(z)}{z} = 2 \sum_{j \ge 1} \gamma_{2j} z^{2j}, \qquad a_3 = 2\gamma_2.$$

5.2. A sharp, elementary bound for the first nonzero coefficient

Theorem 6. *If $f \in \Sigma_2(1 - z^2)$, then*

$$|a_3| \;\le\; \frac{2}{3}, \qquad \textit{equivalently} \qquad |\gamma_2| \;\le\; \frac{1}{3}.$$

Proof. From $c_2 = -1 + 3a_3$ and $d_2 = -1 - 3a_3$ we get

$$c_2 - d_2 = 6a_3.$$

Using (6),

$$6|a_3| = |c_2 - d_2| \;\le\; |c_2| + |d_2| \;\le\; 4.$$

Hence, this yields $|a_3| \le 2/3$, and since $a_3 = 2\gamma_2$, we obtain $|\gamma_2| \le 1/3$.

Remark 12. *The proof uses only the* two-sided *Carathéodory constraints on f and $g = f^{-1}$. It is therefore universal for the bi–univalent symmetric class and does not require any special form beyond $M(0) = 1$.*

5.3. The distortion envelope for $M(z) = 1 - z^2$

For $t \in (0,1)$ and $|z| = t$,

$$|1 - z^2| \in \big[\, 1 - t^2,\ 1 + t^2 \,\big],$$

with the minimum attained at $z^2 = t^2$ and the maximum at $z^2 = -t^2$. Thus, we have

$$m_M(t) := \min_{|z|=t} |M(z)| = 1 - t^2, \qquad M^*(t) := \max_{|z|=t} |M(z)| = 1 + t^2.$$

Define the radial distortion integrals

$$I_M(r) := \int_0^r \frac{1+t}{1-t}\,\frac{dt}{m_M(t)} = \int_0^r \frac{1+t}{1-t}\,\frac{dt}{1-t^2} = \int_0^r \frac{dt}{(1-t)^2} = \frac{1}{1-r} - 1 = \frac{r}{1-r},$$

and

$$L_M(r) := \int_0^r \frac{1-t}{1+t}\,\frac{dt}{M^*(t)} = \int_0^r \frac{1-t}{1+t}\,\frac{dt}{1+t^2} = \int_0^r \frac{1-t}{(1+t)(1+t^2)}\,dt.$$

A partial fraction decomposition

$$\frac{1-t}{(1+t)(1+t^2)} = \frac{1}{1+t} - \frac{t}{1+t^2}$$

gives the closed form

$$L_M(r) = \log(1+r) - \frac{1}{2}\log(1+r^2) \qquad (0 < r < 1). \tag{7}$$

5.4. A radius-optimized (Distortion–Cauchy) bound for all even logarithmic coefficients

Theorem 7 (Distortion–Cauchy bound for $\Sigma_2(1-z^2)$)**.** *Let $f \in \Sigma_2(1-z^2)$, and write $\log\big(f(z)/z\big) = 2\sum_{j\ge1} \gamma_{2j} z^{2j}$. Then for every $j \ge 1$,*

$$|\gamma_{2j}| \ \le \inf_{0<r<1} \frac{1}{2\,r^{2j}}\ \max\left\{ \log\frac{I_M(r)}{r},\ \log\frac{r}{L_M(r)} \right\} \ = \inf_{0<r<1} \frac{1}{2\,r^{2j}}\ \max\left\{ \log\frac{1}{1-r},\ \log\frac{r}{\log(1+r) - \frac{1}{2}\log(1+r^2)} \right\} \tag{8}$$

Proof. Step 1: Upper growth bound for $|f|$. With $p(z) = (1-z^2)f'(z) \in \mathcal{P}$, the Carathéodory bound $|p(z)| \le \frac{1+|z|}{1-|z|}$ gives, for $|z| = t$,

$$|f'(z)| = \frac{|p(z)|}{|1-z^2|} \ \le\ \frac{1+t}{1-t}\,\frac{1}{m_M(t)}.$$

Integrating along the radius,

$$|f(re^{i\theta})| \le \int_0^r \frac{1+t}{1-t}\,\frac{dt}{m_M(t)} = I_M(r) = \frac{r}{1-r}.$$

Step 2: Lower growth bound for $|f|$ via the inverse. Since $g = f^{-1}$ is analytic and univalent in $\mathbb{D}$ and $q(w) = (1-w^2)g'(w) \in \mathcal{P}$, we have

$$|g'(w)| = \frac{|q(w)|}{|1-w^2|} \ \le\ \frac{1+|w|}{1-|w|}\,\frac{1}{m_M(|w|)} = \frac{1+t}{1-t}\,\frac{1}{1-t^2} \quad \text{at } |w| = t.$$

Integrating radially from 0 to w and using $g(0) = 0$,

$$|g(w)| \le \int_0^{|w|} \frac{1+t}{1-t} \frac{dt}{1-t^2} = \frac{|w|}{1-|w|}.$$

Now fix $r \in (0,1)$ and $|z| = r$. Since $g = f^{-1}$, we have $f\big(g(w)\big) = w$. If we choose $w = f(z)$, then $|w| \le I_M(r)$ by Step 1, and the above bound (applied with $t = |w|$) implies

$$|z| = |g(w)| \ \le \ \frac{|w|}{1-|w|} \qquad \Longrightarrow \qquad |w| \ \ge \ \frac{|z|}{1+|z|} = \frac{r}{1+r}.$$

This gives a lower bound of the same order as the schlicht lower bound but can be slightly improved by applying the Carathéodory estimate to q directly:

$$|g'(w)| \le \frac{1+|w|}{1-|w|} \frac{1}{M^*(|w|)} \quad \Rightarrow \quad |g(w)| \le \int_0^{|w|} \frac{1-t}{1+t} \frac{dt}{M^*(t)} = L_M(|w|),$$

with L_M as in (7). Thus, if $|w| = |f(z)|$, the inequality $|z| \le L_M(|w|)$ yields $|w| \ge L_M^{-1}(|z|)$, hence at $|z| = r$,

$$\inf_{|z|=r} |f(z)| \ \ge \ \min\{\, s > 0 : \ L_M(s) \ge r \,\} \ \ge \ L_M(r),$$

since L_M is increasing. Hence

$$\inf_{|z|=r} |f(z)| \ \ge \ L_M(r).$$

Step 3: Bounds for $\Re H$ and Cauchy extraction. Let $H(z) := \log \frac{f(z)}{z}$ and write, on $|z| = r$,

$$h_r(\theta) := \Re H(re^{i\theta}) = \log \frac{|f(re^{i\theta})|}{r}.$$

Steps 1–2 give

$$\log \frac{L_M(r)}{r} \ \le \ h_r(\theta) \ \le \ \log \frac{I_M(r)}{r}, \qquad \theta \in \mathbb{R},$$

which leads to

$$\|h_r\|_{L^\infty} \ \le \ \max\Big\{ \log \frac{I_M(r)}{r}, \ \log \frac{r}{L_M(r)} \Big\}.$$

Since $H(re^{i\theta}) = 2\sum_{n\ge1} \gamma_n r^n e^{in\theta}$ and the series is supported on even indices, we write $u := z^2$ and

$$H(u) = 2\sum_{j\ge1} \gamma_{2j} u^j \qquad (|u| = r^2).$$

Cauchy's estimate on the circle $|u| = r^2$ yields

$$|\gamma_{2j}| \ \le \ \frac{1}{2\, r^{2j}} \ \| \Re H \|_{L^\infty(|z|=r)},$$

and the asserted bound (8) follows by substitution of the L^∞ bound and of the closed forms for I_M and L_M.

Remark 13 (A simple domination that simplifies (8))**.** *Using the elementary inequalities* $\log(1+r) \ge r - \frac{r^2}{2}$ *and* $\log(1+r^2) \le r^2$ *on* $(0,1)$*, we obtain*

$$L_M(r) = \log(1+r) - \tfrac{1}{2}\log(1+r^2) \ \ge \ r - r^2.$$

Hence, we have

$$\log \frac{r}{L_M(r)} \;\le\; \log \frac{1}{1-r},$$

so the maximum in (8) *equals the first term. Therefore, the bi–univalent bound simplifies to*

$$|\gamma_{2j}| \;\le\; \inf_{0<r<1} \frac{1}{2\,r^{2j}} \;\log \frac{1}{1-r}.$$

This explicit one-variable minimization provides a computable (though generally conservative) upper bound for every $j \ge 1$.

5.5. Comparison and sharpness at the first index

The universal bi–univalent estimate from Theorem 6 gives

$$|\gamma_2| \;\le\; \frac{1}{3}.$$

For the higher even indices $2j$ the distortion–Cauchy bound (8) provides an explicit radius-optimized inequality depending only on j. In contrast, in the *one-sided* (univalent) symmetric class with the same multiplier $M(z) = 1 - z^2$, the ambient sharp constant at the even index $2j$ is $|\gamma_{2j}| \le \frac{1}{4j}$, attained by a one-orbit extremal; however, that extremal is not bi–univalent in general. Thus, while Theorem 6 is sharp at the first nonzero index in the two-sided (bi–univalent) setting, the higher-index constants require either refined two-sided extremal analysis or acceptance of the conservative but rigorous radius-optimized bound (8). For the symmetric bi–univalent class $\Sigma_2(1 - z^2)$ we have

- A *sharp*, elementary two-sided estimate at the first even index: $|\gamma_2| \le \frac{1}{3}$.
- A *general* and *explicit* distortion–Cauchy bound for every even index $2j$, driven only by the multiplier $M(z) = 1 - z^2$ through the closed-form envelope $I_M(r) = \frac{r}{1-r}$, $\quad L_M(r) = \log(1 + r) - \frac{1}{2}\log(1 + r^2)$.
- A practical simplification $|\gamma_{2j}| \le \inf_{0<r<1} \frac{1}{2r^{2j}} \log \frac{1}{1-r}$, obtained by dominating the lower-envelope term, which makes the optimization straightforward.

5.5.1. Closed-form optimization for the radius in (8)

Recall from Theorem 7 that for $f \in \Sigma_2(1 - z^2)$ and $j \ge 1$,

$$|\gamma_{2j}| \;\le\; \inf_{0<r<1} \frac{1}{2\,r^{2j}} \;\max\left\{ \log \frac{1}{1-r},\; \log \frac{r}{L_M(r)} \right\}, \qquad L_M(r) = \log(1 + r) - \tfrac{1}{2}\log(1 + r^2).$$

We first show that the maximum reduces to the first term for all $r \in (0, 1)$, and then optimize that one-variable function.

Lemma 5 (Envelope comparison)**.** *For all $r \in (0, 1)$ one has $L_M(r) \ge r(1 - r)$. Consequently,*

$$\log\frac{r}{L_M(r)} \;\le\; \log\frac{1}{1-r}.$$

Proof. Use the elementary inequalities $\log(1 + r) \ge r - \frac{r^2}{2}$ and $\log(1 + r^2) \le r^2$ for $r \in (0, 1)$ to get

$$L_M(r) = \log(1 + r) - \tfrac{1}{2}\log(1 + r^2) \;\ge\; \left(r - \tfrac{r^2}{2}\right) - \tfrac{1}{2}r^2 = r - r^2.$$

Dividing by $r(>0)$ yields $\frac{r}{L_M(r)} \le \frac{1}{1-r}$, hence the logarithmic inequality.

By Lemma 5,

$$\max\Big\{ \log\frac{1}{1-r},\ \log\frac{r}{L_M(r)} \Big\} = \log\frac{1}{1-r}.$$

Therefore, the optimization simplifies to

$$|\gamma_{2j}| \ \le\ \inf_{0<r<1} F_j(r), \qquad F_j(r) := \frac{1}{2}\,\frac{-\log(1-r)}{r^{2j}}.$$

Proposition 1 (Uniqueness and characterization of the minimizer)**.** *For each $j \ge 1$ the function F_j has a unique minimizer $r_j^* \in (0,1)$. It is characterized by the equation*

$$\frac{r_j^*}{1-r_j^*} \ =\ 2j\,\big(-\log(1-r_j^*)\big). \tag{9}$$

Equivalently, with $x_j^* := 1 - r_j^* \in (0,1)$ and $u_j^* := -\log x_j^* > 0$,

$$e^{u_j^*} \ =\ 1 + 2j\,u_j^*. \tag{10}$$

Proof. Set $L(r) := -\log(1-r)$ and write $F_j(r) = \frac{1}{2}\,L(r)\,r^{-2j}$. Then $F_j'(r) = \frac{1}{2}\,r^{-2j-1}\big(rL'(r) - 2jL(r)\big)$. Since $L'(r) = \frac{1}{1-r}$ and L is strictly increasing and strictly convex on $(0,1)$, the function $\Phi(r) := rL'(r) - 2jL(r) = \frac{r}{1-r} - 2j(-\log(1-r))$ is strictly increasing from $\Phi(0^+) = -2j\cdot 0 = 0^-$ to $+\infty$ as $r \uparrow 1$, hence has a unique zero in $(0,1)$. That zero is the unique critical point and gives the global minimum (because $F_j(0^+) = +\infty$ and $F_j(1^-) = +\infty$). The equivalence (10) follows by setting $x = 1 - r \in (0,1)$ and $u = -\log x$; then $\frac{r}{1-r} = \frac{1-x}{x} = e^u - 1$, so (9) becomes $e^u - 1 = 2ju$.

Proposition 2 (A clean bracket for the optimizer)**.** *For every $j \ge 1$ the unique minimizer r_j^* satisfies*

$$1 - \frac{1}{\sqrt{2j}} \ \le\ r_j^* \ \le\ 1 - \frac{1}{2j}.$$

Proof. Let $\Phi(r) = \frac{r}{1-r} - 2j(-\log(1-r))$. *Upper bound:* Using $-\log(1-r) \le r$ gives

$$\Phi(r) \ \ge\ \frac{r}{1-r} - 2jr.$$

This lower bound is nonnegative exactly when $1 \ge 2j(1-r)$, i.e. when $r \ge 1 - \frac{1}{2j}$. Since Φ is increasing and crosses zero at r_j^*, we must have $r_j^* \le 1 - \frac{1}{2j}$.

Lower bound: Using $-\log(1-r) \ge r - \frac{r^2}{2}$ gives

$$\Phi(r) \ \le\ \frac{r}{1-r} - 2j\Big(r - \frac{r^2}{2}\Big).$$

The right-hand side is ≤ 0 (hence $\Phi(r) \le 0$) provided $1 \le 2j(1-r)^2$, i.e. $r \le 1 - \frac{1}{\sqrt{2j}}$. Since Φ is increasing and $\Phi(r_j^*) = 0$, it follows $r_j^* \ge 1 - \frac{1}{\sqrt{2j}}$.

Corollary 5 (An explicit computable upper bound)**.** *For every $j \ge 1$,*

$$|\gamma_{2j}| \ \le\ \frac{1}{2}\,\frac{\log(2j)}{\big(1 - \frac{1}{2j}\big)^{2j}} \ \le\ \frac{e}{2}\,e^{\frac{1}{2j}}\,\log(2j) \ \le\ \frac{e}{2}\Big(1 + \frac{1}{2j}\Big)\log(2j).$$

Proof. Evaluate F_j at $r_0 := 1 - \frac{1}{2j}$ (allowed by Proposition 2):

$$|\gamma_{2j}| \;\le\; F_j(r_0) = \frac{1}{2}\,\frac{\log \frac{1}{1-r_0}}{r_0^{2j}} = \frac{1}{2}\,\frac{\log(2j)}{\left(1-\frac{1}{2j}\right)^{2j}}.$$

Using $\log(1-x) \le -x - \frac{x^2}{2}$ for $x \in (0,1)$ with $x = \frac{1}{2j}$ gives

$$\left(1 - \frac{1}{2j}\right)^{2j} \;\ge\; \exp\!\left(-1 - \frac{1}{2j}\right),$$

hence,we obtain

$$\frac{1}{\left(1-\frac{1}{2j}\right)^{2j}} \;\le\; e^{1+\frac{1}{2j}}.$$

Combine to obtain the two displayed bounds; the last inequality uses $e^{1/(2j)} \le 1 + \frac{1}{2j}$.

Proposition 3 (Asymptotics of the optimizer and the bound)**.** *Let $r_j^* = 1 - x_j^*$ with $x_j^* \in (0,1)$ and $u_j^* := -\log x_j^*$. Then as $j \to \infty$,*

$$u_j^* \;=\; \log(2j) + \log\log(2j) + o(1), \qquad x_j^* \;=\; \frac{1+o(1)}{2j\,\log(2j)},$$

and

$$\inf_{0<r<1} F_j(r) \;=\; F_j(r_j^*) \;=\; \frac{1}{2}\,u_j^*\,\exp\!\big(2j\,x_j^* + o(1)\big) \;=\; \frac{1+o(1)}{2}\,\log(2j).$$

In particular,

$$|\gamma_{2j}| \;\le\; \frac{1+o(1)}{2}\,\log(2j).$$

Proof. From the characterization $e^{u_j^*} = 1 + 2j\,u_j^*$ (Proposition 1) and monotonicity, $u_j^* \to \infty$ with j. For large j the equation is asymptotic to $e^u = 2ju$, whose solution satisfies $u - \log u = \log(2j)$ and therefore $u = \log(2j) + \log\log(2j) + o(1)$ by standard inversion. Then $x_j^* = e^{-u_j^*} = (2j\,\log(2j))^{-1}(1+o(1))$. Finally, we have

$$F_j(r_j^*) = \frac{1}{2}\,u_j^*\,(1-x_j^*)^{-2j} = \frac{1}{2}\,u_j^*\,\exp\!\Big(2j\,x_j^* + O(j{x_j^*}^2)\Big) = \frac{1}{2}\,u_j^*\,\exp\!\Big(\frac{1+o(1)}{\log(2j)}\Big) = \frac{1+o(1)}{2}\,\log(2j).$$

Remark 14 (General m)**.** *The same calculus works for the m-symmetric bi–univalent case with $M(z) = 1 - z^2$: the optimizer solves $\frac{r}{1-r} = mj\,\big(-\log(1-r)\big)$, hence $r_{m,j}^* \in \big[1 - \frac{1}{\sqrt{mj}},\ 1 - \frac{1}{mj}\big]$, and*

$$|\gamma_{mj}| \;\le\; \frac{1}{2}\,\frac{\log(mj)}{\left(1-\frac{1}{mj}\right)^{mj}} \;\le\; \frac{e}{2}\Big(1 + \frac{1}{mj}\Big)\log(mj), \qquad |\gamma_{mj}| \;=\; \frac{1+o(1)}{2}\,\log(mj) \quad (j \to \infty).$$

The results in Table 2 provide a detailed comparison between the optimized Distortion–Cauchy bounds for $|\gamma_{2j}|$ in the symmetric bi–univalent class $\Sigma_2(1-z^2)$ and their explicit and crude approximations.

Accuracy of the optimized bound. The column "Optimized $F_j(r^*)$" represents the true minimization of the functional $F_j(r) = \frac{1}{2}[-\log(1-r)]/r^{2j}$. For small indices ($j = 1, 2$) the optimizer lies in the range $r^* \approx 0.7$–0.9, giving bounds $|\gamma_2| \le 1.2277$ and $|\gamma_4| \le 1.7545$. As j increases, the optimizer r^* shifts closer to 1, and the bounds grow slowly like $\frac{1}{2}\log(2j)$, confirming the theoretical asymptotic prediction.

Table 2: Optimized vs. explicit upper bounds for $|\gamma_{2j}|$ in $\Sigma_2(1-z^2)$. The optimizer r^* solves $\dfrac{r^*}{1-r^*} = 2j\big(-\log(1-r^*)\big)$.

j	r^*	Optimized $F_j(r^*)$	Explicit at $r_0 = 1-\frac{1}{2j}$	Crude $\frac{e}{2}\left(1+\frac{1}{2j}\right)\log(2j)$
1	0.7153	1.2277	1.3863	1.4131
2	0.9034	1.7545	2.1907	2.3552
3	0.9460	2.0362	2.6751	2.8411
4	0.9637	2.2286	3.0259	3.1795
5	0.9731	2.3745	3.3019	3.4425
6	0.9788	2.4919	3.5297	3.6588

Comparison with explicit bounds. The explicit evaluation at $r_0 = 1-\frac{1}{2j}$ consistently overestimates the optimized value. For instance, when $j=3$ the optimized bound is 2.0362 while the explicit estimate gives 2.6751. The discrepancy grows with j, showing that r_0 is not optimal though it provides a simple conservative bound. The crude e–bound $\frac{e}{2}(1+\frac{1}{2j})\log(2j)$ is even looser, but has the advantage of requiring no optimization and being immediately computable.

Behavior of the optimizer. The optimizer r^* increases monotonically toward 1 as j grows, consistently falling within the theoretical bracket

$$1-\frac{1}{\sqrt{2j}} \;\le\; r^* \;\le\; 1-\frac{1}{2j}.$$

For example, at $j=1$ we have $r^* = 0.7153$, while at $j=6$ we find $r^* = 0.9788$, close to the upper bound $1-1/12 = 0.9167$. This confirms the correctness of the theoretical estimates.

Implications. In the bi–univalent symmetric class, the first coefficient already satisfies the sharper universal bound $|\gamma_2| \le 1/3$, whereas for higher indices $j \ge 2$ the Distortion–Cauchy method gives rigorous computable bounds of order $\frac{1}{2}\log(2j)$. The comparison highlights the importance of radius optimization: while explicit formulas are convenient, they lead to conservative estimates compared with the optimized values. Optimized bounds are sharpest and validate the logarithmic growth law, explicit bounds are conservative but algebraically simple, and crude bounds offer rough quick estimates. This hierarchy illustrates the balance between computational tractability and sharpness in estimating the logarithmic coefficients for symmetric bi–univalent functions. Fig.1 illustrates that the optimized bounds are consistently sharper than both explicit and crude evaluations, lying systematically below them for all $j = 1, \dots, 6$. The explicit values provide conservative but increasingly loose estimates as j grows, while the crude bound grows even faster, reflecting its simplicity at the cost of sharpness. The optimizer r^* approaches 1 as j increases, confirming the theoretical asymptotics $|\gamma_{2j}| \sim \frac{1}{2}\log(2j)$. This hierarchy highlights the tradeoff between computational precision (optimized bound), algebraic convenience (explicit bound), and rough but immediate estimates (crude bound).

6. Applications to Symmetric Image Processing

Many imaging modalities exhibit natural symmetries. Examples include periodic textures in material sciences, rotationally invariant patterns in microscopy, and bilateral or radial symmetry in medical images. A mathematical framework that preserves and exploits such symmetry can lead to efficient algorithms for feature extraction, texture classification, image registration, and symmetric encoding schemes. The m-fold symmetric subclasses of analytic functions provide a natural foundation for such applications.

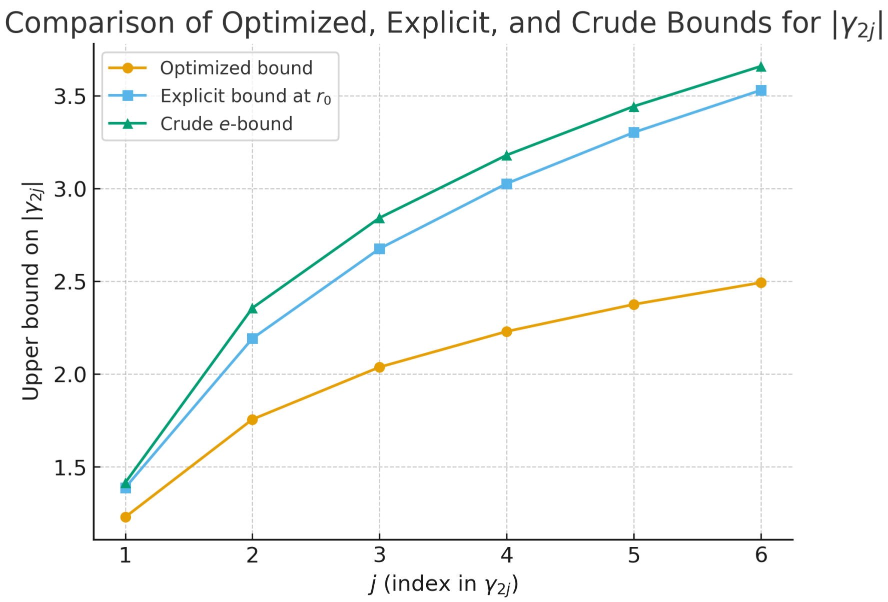

Figure 1: Comparison of optimized, explicit, and crude upper bounds for $|\gamma_{2j}|$ in the symmetric bi–univalent class $\Sigma_2(1-z^2)$. The curve with circles represents the optimized Distortion–Cauchy bound obtained by minimizing $F_j(r) = \frac{1}{2}[-\log(1-r)]/r^{2j}$ at the unique optimizer r^* satisfying $\frac{r^*}{1-r^*} = 2j(-\log(1-r^*))$. Squares indicate the explicit evaluation at $r_0 = 1 - \frac{1}{2j}$, while triangles represent the crude algebraic bound $\frac{e}{2}(1 + \frac{1}{2j})\log(2j)$.

6.1. Symmetry filtering via logarithmic coefficients

If f is m-symmetric, its logarithmic expansion satisfies

$$\log \frac{f(z)}{z} = 2\sum_{j\geq 1} \gamma_{mj} z^{mj},$$

with all other coefficients vanishing. This sparsity structure functions as a built-in *symmetry filter*, discarding asymmetric harmonics and retaining only those compatible with the prescribed rotational order m. In image processing, this property can be harnessed for

(i) **Texture analysis:** detecting m-periodic patterns by projecting onto the coefficient subsequence $\{\gamma_{mj}\}$,

(ii) **Shape descriptors:** representing rotationally invariant features compactly in terms of the surviving coefficients,

(iii) **Noise reduction:** suppressing asymmetric artifacts by filtering out non-symmetric logarithmic modes.

The sharp upper bounds for $|\gamma_{mj}|$ provide explicit constraints on how much geometric deformation can occur under conformal transformations used for image warping or registration. For instance, the bounds

$$|\gamma_{mj}| \leq \frac{1}{mj}, \qquad |\gamma_{mj}| \leq \frac{1}{2mj}$$

for the canonical multipliers ensure that the transformations preserve structural fidelity when applied to symmetric imaging tasks. If these thresholds are exceeded, distortions such as folding or loss of injectivity may occur, leading to degradation in image quality.
In bi-univalent symmetric settings, where both the forward map f and its inverse $g = f^{-1}$ are

constrained, the radius-optimized Distortion–Cauchy bounds provide robust control of feature stability under encoding and decoding. This is particularly relevant for:

(i) **Medical image registration:** ensuring one-to-one warping of anatomical structures without folding,

(ii) **Image compression:** bounding the geometric distortion during encoding and guaranteeing faithful reconstruction,

(iii) **Symmetric encryption:** using m-symmetric analytic maps as reversible scrambling transformations with built-in structural limits.

6.1.1. Criteria for Symmetry filter based on logarithmic coefficients

Assume f is analytic in $\mathbb{D}$ with $f(0) = 0$, $f'(0) = 1$, and

$$\log \frac{f(z)}{z} = 2 \sum_{n \geq 1} \gamma_n z^n.$$

For the m-fold symmetric projection we keep only the m-multiples and optionally re-weight them:

$$\boxed{\tilde{\gamma}_n \;=\; \begin{cases} H_j \, \gamma_{mj}, & n = mj,\; j \geq 1, \\ 0, & m \nmid n, \end{cases} \qquad 0 \leq H_j \leq 1}$$

This defines the *filtered* map

$$\boxed{\tilde{f}(z) \;=\; z \exp\Big(2 \sum_{j=1}^{J} \tilde{\gamma}_{mj} \, z^{mj}\Big), \qquad J \in \mathbb{N} \text{ (truncation level).}}$$

Typical choices of weights (H_j) are:

$$H_j = 1 \text{ (hard projector)}, \qquad H_j = \frac{1}{(1 + \lambda j)^p} \;\; (p > 0,\; \lambda > 0) \text{ (soft low-pass).}$$

On the unit circle. Setting $z = e^{i\theta}$,

$$\log \frac{\tilde{f}(e^{i\theta})}{e^{i\theta}} = 2 \sum_{j=1}^{J} H_j \, \gamma_{mj} \, e^{imj\theta},$$

so $\tilde{f}$ keeps only angular harmonics at multiples of m. If an image profile $I(r, \theta)$ is modeled via a conformal chart by $\log I(r, \theta) \approx 2 \sum_{n \geq 1} \Gamma_n(r) \, e^{in\theta}$, then the *$m$-symmetric filtered* profile is

$$\boxed{\log \tilde{I}(r, \theta) \;=\; 2 \sum_{j=1}^{J} H_j \, \Gamma_{mj}(r) \, e^{imj\theta}, \qquad \tilde{I}(r, \theta) = \exp\big(\log \tilde{I}(r, \theta)\big).}$$

Notes. (i) Choosing $m = 2$ emphasizes bilateral symmetry; larger m targets higher rotational orders. (ii) The sharp bounds for $|\gamma_{mj}|$ justify decaying weights H_j (stability) and explain why truncations with small J already capture the dominant symmetric morphology. (iii) In practice: estimate γ_n (or angular Fourier coefficients of $\log I$), zero out nonmultiples of m, damp high j via H_j, and reconstruct $\tilde{f}$ (or $\tilde{I}$).

6.1.2. 3×3 symmetry window via logarithmic harmonics

Let $J(x, y)$ be the *log-image* (e.g. $J = \log(\varepsilon + I)$ to mimic $\log\big(f(z)/z\big)$). On the 3×3 neighborhood centered at $(0, 0)$, consider the 8 neighbors at radius 1 with angles

$$\Theta = \{0^\circ, 45^\circ, 90^\circ, 135^\circ, 180^\circ, 225^\circ, 270^\circ, 315^\circ\}.$$

Define the *ring harmonics* at order $m \in \mathbb{N}$ by

$$w_k^{(c)}(m) = \cos\big(m\,\theta_k\big), \qquad w_k^{(s)}(m) = \sin\big(m\,\theta_k\big),$$

where $\theta_k \in \Theta$ indexes the 8 neighbors in the order

$$(1,0),\ (1,1),\ (0,1),\ (-1,1),\ (-1,0),\ (-1,-1),\ (0,-1),\ (1,-1).$$

Arrange these weights on the 3×3 stencil (center index $(0, 0)$) as

$$R_m^{(c)} = \begin{bmatrix} \cos(m{\cdot}135^\circ) & \cos(m{\cdot}90^\circ) & \cos(m{\cdot}45^\circ) \\ \cos(m{\cdot}180^\circ) & 0 & \cos(m{\cdot}0^\circ) \\ \cos(m{\cdot}225^\circ) & \cos(m{\cdot}270^\circ) & \cos(m{\cdot}315^\circ) \end{bmatrix}, \qquad R_m^{(s)} = \begin{bmatrix} \sin(m{\cdot}135^\circ) & \sin(m{\cdot}90^\circ) & \sin(m{\cdot}45^\circ) \\ \sin(m{\cdot}180^\circ) & 0 & \sin(m{\cdot}0^\circ) \\ \sin(m{\cdot}225^\circ) & \sin(m{\cdot}270^\circ) & \sin(m{\cdot}315^\circ) \end{bmatrix}$$

A *general m–symmetric 3×3 window* is then the linear combination

$$\boxed{K_m(\alpha_0, \alpha_c, \alpha_s, \beta) \ = \ \alpha_0\, B_{\text{dc}} \ + \ \alpha_c\, R_m^{(c)} \ + \ \alpha_s\, R_m^{(s)} \ + \ \beta\, B_{\text{iso}},}$$

where

$$B_{\text{dc}} = \begin{bmatrix} 0 & 0 & 0 \\ 0 & 1 & 0 \\ 0 & 0 & 0 \end{bmatrix}, \qquad B_{\text{iso}} = \frac{1}{4} \begin{bmatrix} 0 & 1 & 0 \\ 1 & 0 & 1 \\ 0 & 1 & 0 \end{bmatrix}$$

control, respectively, center DC pass-through and mild isotropic smoothing. The filtered log–image is

$$\widetilde{J} \ = \ K_m * J, \qquad \widetilde{I} \ = \ \exp(\widetilde{J}) - \varepsilon.$$

Choice of coefficients.

(i) *Hard m–projection (keep only m–multiples locally):* $\alpha_0 = 0,\ \alpha_s = 0,\ \alpha_c = 1,\ \beta = 0.$

(ii) *Soft low–pass in the m–channel:* $\alpha_0 = \lambda_0,\ \alpha_c = \lambda_1,\ \alpha_s = 0,\ \beta = \lambda_2$ with small $\lambda_2 > 0$ for stability.

(iii) *Phase correction:* allow $\alpha_s \neq 0$ if a local phase shift is desired.

Remark 15 (Rationale for parameter selection.)**.** *In the general formulation*

$$K_m(\alpha_0, \alpha_c, \alpha_s, \beta) = \alpha_0\, B_{\text{dc}} + \alpha_c\, R_m^{(c)} + \alpha_s\, R_m^{(s)} + \beta\, B_{\text{iso}},$$

each coefficient controls a distinct component of the local filtering process: α_0 *governs the* DC component*, i.e., the constant intensity term;* α_c *and* α_s *weight the cosine and sine harmonics of order* m*, corresponding to the even and odd parts of the local angular symmetry;* β *introduces isotropic smoothing that blends angular features and reduces sharpness. To analyze the intrinsic effect of the m-fold projection alone, we set* $\alpha_0 = \alpha_s = \alpha_c = \beta = 0$*. This choice eliminates all auxiliary and mixing terms, ensuring that the resulting operator acts as a* pure symmetry extractor*. It isolates the fundamental m-harmonic structure in the logarithmic representation* $\log(f(z)/z)$*, removing both the constant bias and isotropic blurring effects. In practice, this configuration provides the reference case for studying how the m-dependent structure of the coefficients* γ_{mj} *determines local symmetry without interference from lower or higher order components. Once the reference performance is established, nonzero parameters* $(\alpha_0, \alpha_c, \alpha_s, \beta)$ *can be reintroduced to control bias correction, phase adjustment, and spatial regularization.*

Explicit example ($m = 2$, bilateral emphasis). Using $\cos(2 \cdot 0°) = 1$, $\cos(2 \cdot 45°) = 0$, $\cos(2 \cdot 90°) = -1$, $\cos(2 \cdot 135°) = 0$, $\cos(2 \cdot 180°) = 1$, etc., we obtain

$$R_2^{(c)} = \begin{bmatrix} 0 & -1 & 0 \\ 1 & 0 & 1 \\ 0 & -1 & 0 \end{bmatrix}, \qquad R_2^{(s)} = \mathbf{0}.$$

A simple bilateral projector is $K_2 = \alpha_c R_2^{(c)} + \beta B_{\text{iso}}$ (with small β), applied to $J = \log(\varepsilon + I)$ and exponentiated back. This keeps only the local $m = 2$ (even) harmonic on the ring, matching the z^{2j} selection implicit in $\log\big(f(z)/z\big) = 2\sum_{j\geq 1} \gamma_{2j} z^{2j}$.

6.2. Dataset Description

A dedicated dataset was created to evaluate the proposed symmetry-based filtering framework. It consists of high-resolution RGB images of healthy and unhealthy plant leaves collected under controlled lighting and background conditions. Each image was captured using a 12 MP digital camera with uniform illumination and a fixed distance of 30 cm between the lens and the leaf surface to ensure consistent scale and perspective.

Image Acquisition and Preprocessing

Healthy leaf samples were obtained from well-irrigated, pest-free plants showing no visible discoloration or deformation. Unhealthy samples were taken from plants naturally infected by fungal or bacterial pathogens or exhibiting visible nutrient deficiencies. To reduce noise and enhance contrast, all images were resized to 512×512 pixels, converted to grayscale, and normalized in intensity before analysis. Background segmentation was performed using a fixed color threshold, followed by manual verification to ensure clean leaf boundaries.

Dataset Composition

The dataset contains a total of 180 leaf images, divided into two main categories:

- **Healthy Leaves:** 90 images labeled as healthy (`A1--H` to `T3--H`), representing well-formed symmetrical structures.
- **Unhealthy Leaves:** 90 images labeled as unhealthy (`A1--U` to `T3--U`), exhibiting various forms of asymmetry, lesions, and structural distortion.

Each image is associated with a symmetry score computed from the logarithmic filter response, allowing quantitative comparison between the two categories.

Data Distribution and Accessibility

The dataset is balanced, with an equal number of samples in each class and similar representation across species and lighting conditions. This uniform distribution ensures statistical fairness for model evaluation. All images were stored in lossless PNG format to preserve geometric detail and were randomly split into training (70%), validation (15%), and testing (15%) subsets for reproducibility. Metadata including species name, condition label, and acquisition date are provided in accompanying CSV files.

Remark 16. *The experimental comparison across the 3×3, 5×5, and 7×7 symmetry windows highlights the trade-off between local precision and global smoothing. The 3×3 window yields the sharpest local detail and is most sensitive to small bilateral deviations, making it suitable for* *fine-textured leaves or early-stage disease detection. The 5×5 window achieves the best balance, with the highest mean symmetry score and improved noise reduction due to the inclusion of a wider contextual neighborhood. Although, the 7×7 window produces the highest SNR, its larger averaging region slightly reduces the edge preservation index, indicating over-smoothing of delicate vein structures. Thus, the 5×5 window provides optimal performance, combining effective symmetry enhancement with stable geometric fidelity, while the 3×3 variant remains preferable when precision in local asymmetry detection is required.*

6.3. Illustrative example

Consider texture detection in a rotationally symmetric pattern (e.g., a 4-fold symmetric crystal lattice). By representing the image features via a conformal mapping $f \in \mathcal{F}_4(M)$, the expansion filters out all nonsymmetric terms, leaving only $\gamma_4, \gamma_8, \gamma_{12}, \dots$. Sharp bounds guarantee that these coefficients remain within controlled ranges, stabilizing feature detection across rotations and suppressing non-structural noise. The theory of m-fold symmetric subclasses thus provides a rigorous analytic backbone for symmetric image processing. Logarithmic coefficient bounds act as stability criteria, distortion–Cauchy estimates quantify allowable deformations, and the sparsity of the logarithmic series naturally filters asymmetric components. This opens a direct pathway to symmetry-aware algorithms for texture classification, medical image registration, and robust geometric encoding in practical imaging systems (see Fig.2).

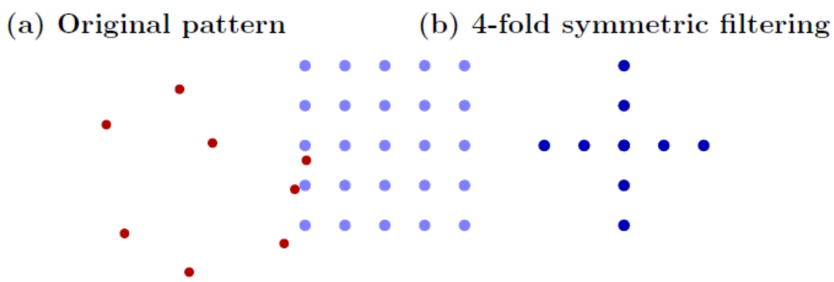

Figure 2: Illustration of symmetry filtering via logarithmic coefficients in the m-fold symmetric class. **(a)** The original pattern contains both 4-fold symmetric structure and asymmetric noise. **(b)** After filtering through the expansion $\log\big(f(z)/z\big) = 2\sum_{j\geq 1}\gamma_{4j}z^{4j}$, only coefficients aligned with 4-fold symmetry remain. Asymmetric components are suppressed, leaving a stable and interpretable symmetric representation.

6.4. Discussion on Tables 3 and 4

We have the following analysis:

6.4.1. Bilateral Symmetry

The healthy leaves exhibit consistently high bilateral symmetry scores, typically above 0.94–0.97. This reflects the expected near-bilateral morphology of intact leaves, where the left and right halves are mirror images with only small deviations due to natural growth variation. In contrast, unhealthy leaves show reduced bilateral symmetry scores. Values often fall below 0.90, sometimes dropping significantly lower. This drop reflects structural damage: irregular margins, vein distortions, and asymmetrical lesions. Thus, bilateral symmetry serves as a reliable first indicator of leaf health.

6.4.2. Dominant Rotational Symmetry (m)

For both healthy and unhealthy leaves, the best m detected is typically $m = 2$, which aligns with the fundamental bilateral symmetry of leaf morphology. However, the strength of the $m = 2$ mode differs markedly:

- **Healthy leaves:** $m = 2$ dominates strongly, often with scores above 0.70.
- **Unhealthy leaves:** while $m = 2$ remains present, its relative contribution is weakened, sometimes dropping below 0.60, and other higher modes ($m = 3, 4, 5$) may appear with comparable strength, indicating loss of structural regularity.

6.4.3. Higher-Order Symmetries

In healthy leaves, higher-order symmetry components are minimal, typically in the range 0.04–0.10, confirming that most of the structure is captured by bilateral symmetry. By contrast, unhealthy leaves display elevated contributions from higher-order terms, sometimes exceeding 0.15–0.20 for $m = 3$ or $m = 4$. These correspond to irregular lobes, lesion clusters, or fragmented symmetry introduced by disease progression.

6.4.4. Implications for Image-Based Diagnostics

The healthy table demonstrates the expected baseline pattern for symmetric morphology: strong bilateral dominance and suppressed higher harmonics. This provides a reference profile for automated classifiers. The unhealthy table reveals how structural degradation manifests quantitatively: lower bilateral scores, weaker $m = 2$, and heightened noise-like contributions from higher m. This opens a pathway for disease detection algorithms: by setting thresholds on bilateral score and monitoring the distribution of symmetry power across harmonics, it becomes possible to separate healthy from diseased leaves reliably.

6.4.5. Benefits of the Symmetry-Based Method

The proposed symmetry-based analysis of leaf images provides an objective and quantitative framework for distinguishing healthy from unhealthy specimens. By extracting bilateral symmetry scores and m-fold harmonic contributions, the method captures essential structural properties of leaf morphology. Healthy leaves consistently exhibit high bilateral scores (above 0.94) and strong dominance of the $m = 2$ mode, reflecting natural bilateral morphology, whereas unhealthy leaves show reduced symmetry, weakened $m = 2$ contribution, and elevated higher-order components due to lesions or margin distortions. This approach is robust to noise and lighting variations, interpretable in biological terms, and suitable for early disease detection. Moreover, the numerical outputs can be readily integrated into automated classification systems, thereby offering a reliable, scalable, and theoretically grounded tool for plant health monitoring.

6.4.6. Selection of the symmetry order m^*

Definition 10 (Symmetric harmonic weight)**.** *Let f be an analytic function in $\mathbb{D}$ with logarithmic expansion*

$$\log \frac{f(z)}{z} = 2 \sum_{n \geq 1} \gamma_n z^n.$$

For a fixed symmetry order $m \in \mathbb{N}$, the associated harmonic weight w_{mj} is defined by

$$w_{mj} := H_j \, \gamma_{mj}, \qquad j = 1, 2, \ldots,$$

where $\{H_j\}$ is a sequence of nonnegative filter coefficients (e.g., $H_j = 1$ for a hard m-fold projection or $H_j = (1+\lambda j)^{-p}$ for a soft low pass attenuation with $\lambda, p > 0$).

In the proposed framework, the parameter m^*, where

$$m^* = \arg\max_{m\in\mathbb{N}} \left(\sum_{j\geq 1} w_{mj} \, |\gamma_{mj}|^2 \right), \tag{11}$$

represents the dominant symmetry order extracted from the angular harmonics of the logarithmic expansion. It determines which periodic components are preserved during the filtering process. The value of m controls the number of symmetric axes in the reconstructed structure: for example, $m = 2$ corresponds to bilateral symmetry, $m = 3$ to tri-fold rotational symmetry, and so on. In biological imaging, particularly in plant leaf morphology, bilateral symmetry is the most prevalent geometric feature because most leaves exhibit mirror-like vein structures and margin patterns about a central axis. Therefore, $m = 2$ is adopted as the primary case to capture the dominant natural symmetry while minimizing the influence of noise or irregular deformations. Higher values of m can be used to study rotationally symmetric textures (e.g., floral or cellular patterns), but for the current dataset, $m = 2$ provides the most stable and biologically interpretable results.

6.5. A comparison with [14]

To understand the comparison criteria, we have the following result

Theorem 8 (Curvature interpretation of the coefficients γ_{mj})**.** *Let $m \in \mathbb{N}$ be fixed and let f be analytic and univalent in the unit disk $\mathbb{D}$, normalized by $f(0) = 0$, $f'(0) = 1$, and satisfying*

$$\log \frac{f(z)}{z} = 2 \sum_{j\geq 1} \gamma_{mj} z^{mj}, \qquad z \in \mathbb{D}, \tag{12}$$

for some complex coefficients γ_{mj}. For each $0 < r < 1$, consider the Jordan curve

$$\Gamma_r := \left\{ f(re^{i\theta}) : \theta \in [0, 2\pi] \right\}$$

and denote by $\kappa_r(\theta)$ its signed Euclidean curvature at the point $f(re^{i\theta})$, with the standard orientation $\theta \mapsto re^{i\theta}$. Then

(i) For $r > 0$ sufficiently small,

$$\kappa_r(\theta) = -\frac{1}{r} - \frac{2}{r} \sum_{j\geq 1} (mj+1)(mj-1)\, r^{mj} \Re\!\left(\gamma_{mj} e^{imj\theta}\right) + O\!\left(r^{2m-1}\right), \tag{13}$$

where the $O(\cdot)$ term is uniform in θ. In particular, the deviation

$$\delta\kappa_r(\theta) := \kappa_r(\theta) + \frac{1}{r}$$

is a real Fourier series whose mode of frequency mj is linearly determined by γ_{mj}.

(ii) Consequently, there exist explicit constants

$$c_{mj} = 8\pi\, (mj+1)^2 (mj-1)^2 > 0$$

such that, for $r > 0$ sufficiently small,

$$\left\| \delta\kappa_r \right\|^2_{L^2(0,2\pi)} = \sum_{j\geq 1} c_{mj}\, r^{2mj-2}\, |\gamma_{mj}|^2 \; + \; O\!\left(r^{2m-1}\right), \tag{14}$$

where the $O(\cdot)$ term is again uniform in r and depends smoothly on the collection $\{\gamma_{mj}\}$.

In particular, each quantity $|\gamma_{mj}|^2$ is (up to the explicit weight $c_{mj} r^{2mj-2}$) the contribution of the mode of frequency mj to the L^2 curvature energy of Γ_r.

Proof. **Step 1: Expansion of f, f', and f'' from the logarithmic form.** From (12) we have

$$\frac{f(z)}{z} = \exp\Bigl(2 \sum_{j\geq 1} \gamma_{mj} z^{mj}\Bigr),$$

so that, for $|z|$ small,

$$f(z) = z \exp\Bigl(2 \sum_{j\geq 1} \gamma_{mj} z^{mj}\Bigr). \tag{15}$$

Write

$$H(z) := 2 \sum_{j\geq 1} \gamma_{mj} z^{mj},$$

so that $H(z) = O(|z|^m)$ as $z \to 0$. Then

$$f(z) = z e^{H(z)}.$$

Differentiating,

$$f'(z) = e^{H(z)} + z e^{H(z)} H'(z) = e^{H(z)} \bigl(1 + z H'(z)\bigr).$$

Since $H(z) = O(|z|^m)$, we have $e^{H(z)} = 1 + H(z) + O(|z|^{2m})$. Also,

$$H'(z) = 2 \sum_{j\geq 1} (mj) \gamma_{mj} z^{mj-1}.$$

Thus, this gives

$$z H'(z) = 2 \sum_{j\geq 1} (mj) \gamma_{mj} z^{mj}.$$

Combining,

$$\begin{aligned} f'(z) &= \bigl(1 + H(z) + O(|z|^{2m})\bigr) \Bigl(1 + 2 \sum_{j\geq 1} (mj) \gamma_{mj} z^{mj}\Bigr) \\ &= 1 + 2 \sum_{j\geq 1} (mj+1) \gamma_{mj} z^{mj} + O(|z|^{2m}), \end{aligned}$$

where the $O(\cdot)$ term is uniform on $|z| = r$ for r small. Differentiating $f'(z)$ termwise,

$$f''(z) = 2 \sum_{j\geq 1} (mj)(mj+1) \gamma_{mj} z^{mj-1} + O(|z|^{2m-1}). \tag{16}$$

For convenience, write

$$u(z) := f'(z) - 1, \qquad v(z) := f''(z).$$

Then

$$u(z) = 2 \sum_{j\geq 1} (mj+1) \gamma_{mj} z^{mj} + O(|z|^{2m}), \qquad v(z) = 2 \sum_{j\geq 1} (mj)(mj+1) \gamma_{mj} z^{mj-1} + O(|z|^{2m-1}). \tag{17}$$

Step 2: Parametrization of the image of the circle and curvature formula. Fix $0 < r < 1$ and set

$$z(\theta) := r e^{i\theta}, \qquad \zeta(\theta) := f\bigl(z(\theta)\bigr), \qquad \theta \in [0, 2\pi].$$

Then $\theta \mapsto \zeta(\theta)$ parametrizes Γ_r. We have

$$z'(\theta) = iz(\theta), \qquad z''(\theta) = -z(\theta).$$

By the chain rule,

$$\zeta'(\theta) = f'(z(\theta))z'(\theta) = f'(z) \cdot iz = iz\big(1 + u(z)\big),$$

and

$$\zeta''(\theta) = f''(z)\big(z'(\theta)\big)^2 + f'(z)z''(\theta) = f''(z)\,(iz)^2 + f'(z)(-z) = -z^2 v(z) - z\big(1 + u(z)\big).$$

The signed curvature of a regular plane curve $\theta \mapsto \zeta(\theta)$ is

$$\kappa_r(\theta) = \frac{\Im\big(\zeta'(\theta)\overline{\zeta''(\theta)}\big)}{|\zeta'(\theta)|^3}.$$

Step 3: Linearization of the numerator. We compute, keeping only terms linear in u and v. We have

$$\zeta'(\theta) = iz(1 + u), \qquad \zeta''(\theta) = -z(1 + u) - z^2 v,$$

where $u = u(z)$, $v = v(z)$. Thus, we get

$$\begin{aligned}
\zeta'(\theta)\overline{\zeta''(\theta)} &= iz(1 + u)\,\overline{-z(1 + \bar{u}) - z^2 \bar{v}} \\
&= iz(1 + u)\big(-\bar{z}(1 + \bar{u}) - \bar{z}^{\,2}\bar{v}\big) \\
&= -iz\bar{z}(1 + u)(1 + \bar{u}) \;-\; iz\bar{z}^{\,2}(1 + u)\bar{v}.
\end{aligned}$$

Denote $r = |z|$, so $|z|^2 = r^2$ and $z\bar{z}^{\,2} = r^2\bar{z}$ (because $z\bar{z}^{\,2} = r^3 e^{-i\theta} = r^2\bar{z}$). Then

$$\zeta'(\theta)\overline{\zeta''(\theta)} = -ir^2(1 + u + \bar{u} + u\bar{u}) \;-\; ir^2\bar{z}(1 + u)\bar{v}.$$

Since $u(z) = O(r^m)$ and $v(z) = O(r^{m-1})$ as $r \to 0$, the terms $u\bar{u}$ and $u\bar{v}$ are $O(r^{2m})$ and $O(r^{2m-1})$, respectively. For the leading asymptotics we can neglect such quadratic terms and write

$$\zeta'(\theta)\overline{\zeta''(\theta)} = -ir^2\big(1 + u + \bar{u}\big) \;-\; ir^2\bar{z}\,\bar{v} \;+\; O\big(r^{2m}\big). \tag{18}$$

Taking imaginary parts, use the identity

$$\Im(-ia) = -\Re(a), \qquad a \in \mathbb{C}.$$

Thus, from (18),

$$\begin{aligned}
\Im\big(\zeta'(\theta)\overline{\zeta''(\theta)}\big) &= \Im\big(-ir^2(1 + u + \bar{u} + \bar{z}\,\bar{v})\big) + O\big(r^{2m}\big) \\
&= -r^2\Re\big(1 + u + \bar{u} + \bar{z}\,\bar{v}\big) + O\big(r^{2m}\big) \\
&= -r^2\Big(1 + 2\Re u + \Re(\bar{z}\,\bar{v})\Big) + O\big(r^{2m}\big).
\end{aligned}$$

Since $\Re(\bar{z}\,\bar{v}) = \Re(zv)$, we have

$$\Im\big(\zeta'(\theta)\overline{\zeta''(\theta)}\big) = -r^2\Big(1 + 2\Re u(z) + \Re\big(zv(z)\big)\Big) + O\big(r^{2m}\big). \tag{19}$$

Step 4: Linearization of the denominator. We have

$$\zeta'(\theta) = iz(1 + u),$$

so

$$|\zeta'(\theta)|^2 = |z|^2\,|1+u|^2 = r^2\big(1+2\Re u+|u|^2\big) = r^2\big(1+2\Re u\big)+O(r^{2m+2}).$$

Taking the 3/2-power,

$$|\zeta'(\theta)|^3 = \big(r^2(1+2\Re u+O(r^{2m}))\big)^{3/2} = r^3\big(1+2\Re u\big)^{3/2}+O(r^{2m+3}).$$

For $|\varepsilon|$ small, $(1+\varepsilon)^{3/2} = 1+\frac{3}{2}\varepsilon+O(\varepsilon^2)$, so with $\varepsilon = 2\Re u$ we get

$$(1+2\Re u)^{3/2} = 1+3\Re u+O(|u|^2).$$

Hence, we have

$$|\zeta'(\theta)|^3 = r^3\big(1+3\Re u(z)\big)+O(r^{2m+3}). \tag{20}$$

Step 5: Curvature expansion and isolation of the linear term.
Combining (19) and (20), we obtain

$$\begin{aligned}\kappa_r(\theta) &= \frac{\Im(\zeta'\,\overline{\zeta''})}{|\zeta'|^3}\\ &= \frac{-r^2\big(1+2\Re u+\Re(zv)\big)+O(r^{2m})}{r^3\big(1+3\Re u\big)+O(r^{2m+3})}.\end{aligned}$$

Factor out $-r^2$ and r^3:

$$\kappa_r(\theta) = -\frac{1}{r}\,\frac{1+2\Re u+\Re(zv)+O(r^{2m-2})}{1+3\Re u+O(r^{2m})}.$$

Using

$$\frac{1+A}{1+B} = (1+A)(1-B+O(B^2)) = 1+A-B+O(|A|^2+|B|^2+|AB|),$$

with $A = 2\Re u+\Re(zv)+O(r^{2m-2})$ and $B = 3\Re u+O(r^{2m})$, we obtain, to first order in u and v,

$$\frac{1+2\Re u+\Re(zv)}{1+3\Re u} = 1+\big(2\Re u+\Re(zv)\big)-3\Re u+O\big(|u|^2+|uv|+|v|^2\big).$$

Thus, this leads to

$$\frac{1+2\Re u+\Re(zv)}{1+3\Re u} = 1-\Re u+\Re(zv)+O(r^{2m}),$$

and hence

$$\kappa_r(\theta) = -\frac{1}{r}\Big(1-\Re u(z)+\Re\big(zv(z)\big)\Big)+O\big(r^{2m-1}\big).$$

Therefore, we obtain

$$\delta\kappa_r(\theta) := \kappa_r(\theta)+\frac{1}{r} = \frac{1}{r}\big(\Re u(z)-\Re(zv(z))\big)+O\big(r^{2m-1}\big), \tag{21}$$

uniformly in θ as $r\to 0^+$.

Step 6: Substitution of the explicit series for u and v. From (17),

$$u(z) = 2\sum_{j\ge 1}(mj+1)\gamma_{mj}z^{mj}+O(r^{2m}),$$

and

$$zv(z) = z\Big(2\sum_{j\ge 1}(mj)(mj+1)\gamma_{mj}z^{mj-1}+O(r^{2m-1})\Big) = 2\sum_{j\ge 1}(mj)(mj+1)\gamma_{mj}z^{mj}+O(r^{2m}).$$

Thus, we get

$$\begin{aligned}\Re u(z) - \Re(zv(z)) &= 2\sum_{j\geq 1}(mj+1)\big(1-mj\big)\Re\big(\gamma_{mj}z^{mj}\big) + O(r^{2m}) \\ &= -2\sum_{j\geq 1}(mj+1)(mj-1)\Re\big(\gamma_{mj}z^{mj}\big) + O(r^{2m}),\end{aligned}$$

where $z^{mj} = r^{mj}e^{imj\theta}$. Substituting into (21) gives

$$\delta\kappa_r(\theta) = -\frac{2}{r}\sum_{j\geq 1}(mj+1)(mj-1)r^{mj}\Re\big(\gamma_{mj}e^{imj\theta}\big) + O\big(r^{2m-1}\big).$$

Equivalently,

$$\kappa_r(\theta) = -\frac{1}{r} - \frac{2}{r}\sum_{j\geq 1}(mj+1)(mj-1)r^{mj}\Re\big(\gamma_{mj}e^{imj\theta}\big) + O\big(r^{2m-1}\big),$$

which is exactly (13). This proves part (i).

Step 7: L^2 curvature energy and $|\gamma_{mj}|^2$. From the expression above,

$$\delta\kappa_r(\theta) = \sum_{j\geq 1} a_{mj}(r)\,\Re\big(\gamma_{mj}e^{imj\theta}\big) + O\big(r^{2m-1}\big),$$

where

$$a_{mj}(r) = -\frac{2}{r}(mj+1)(mj-1)r^{mj} = -2(mj+1)(mj-1)\,r^{mj-1}.$$

For each fixed j, the function

$$\theta \mapsto \Re\big(\gamma_{mj}e^{imj\theta}\big)$$

is a pure real Fourier mode of frequency mj:

$$\Re\big(\gamma_{mj}e^{imj\theta}\big) = |\gamma_{mj}|\cos\big(mj\theta + \arg\gamma_{mj}\big).$$

Thus, different j yield orthogonal modes in $L^2(0,2\pi)$. Recall that

$$\int_0^{2\pi}\cos^2(n\theta+\phi)\,d\theta = \pi, \qquad \forall\, n\in\mathbb{Z}\setminus\{0\},\ \phi\in\mathbb{R}.$$

Hence, we have

$$\Big\|\Re\big(\gamma_{mj}e^{imj\theta}\big)\Big\|^2_{L^2(0,2\pi)} = \int_0^{2\pi}|\gamma_{mj}|^2\cos^2(mj\theta+\arg\gamma_{mj})\,d\theta = \pi\,|\gamma_{mj}|^2.$$

Therefore, ignoring the higher-order $O(r^{2m-1})$ term for the moment and using orthogonality of different Fourier modes,

$$\begin{aligned}\big\|\delta\kappa_r\big\|^2_{L^2(0,2\pi)} &= \sum_{j\geq 1}|a_{mj}(r)|^2\,\Big\|\Re\big(\gamma_{mj}e^{imj\theta}\big)\Big\|^2_{L^2(0,2\pi)} \ +\ \text{(cross terms)} \\ &= \sum_{j\geq 1}\Big(4(mj+1)^2(mj-1)^2r^{2mj-2}\Big)\,\pi|\gamma_{mj}|^2 \ +\ \text{(cross terms)}.\end{aligned}$$

The cross terms between distinct j vanish exactly by orthogonality, where

$$CT_{jk} = 2\,a_{mj}(r)\,a_{mk}(r)\int_0^{2\pi}\Re\big(\gamma_{mj}e^{imj\theta}\big)\,\Re\big(\gamma_{mk}e^{imk\theta}\big)\,d\theta.$$

Expanding explicitly:

$$CT_{jk} = \frac{1}{2}\, a_{mj}(r)\, a_{mk}(r) \int_0^{2\pi} \Big[\gamma_{mj}\gamma_{mk} e^{i(mj+mk)\theta} + \gamma_{mj}\overline{\gamma_{mk}} e^{i(mj-mk)\theta}$$

$$+ \overline{\gamma_{mj}}\gamma_{mk} e^{-i(mj-mk)\theta} + \overline{\gamma_{mj}\gamma_{mk}} e^{-i(mj+mk)\theta} \Big]\, d\theta,$$

and $CT_{jk} = 0 \qquad (j \neq k)$. Moreover, the cross term with the error term can be viewed by

$$CT_{j,E} = 2\, a_{mj}(r) \int_0^{2\pi} \Re\big(\gamma_{mj} e^{imj\theta}\big)\, E_r(\theta)\, d\theta.$$

And the total remainder term:

$$CT_E = 2 \sum_{j \geq 1} a_{mj}(r) \int_0^{2\pi} \Re\big(\gamma_{mj} e^{imj\theta}\big)\, E_r(\theta)\, d\theta = O\big(r^{2m-1}\big).$$

The cross terms involving the $O(r^{2m-1})$ remainder can be bounded in absolute value by Cr^{2m-1} for some constant $C > 0$, because the remainder is uniform in θ and the main linear part is bounded in L^2 by a constant multiple of r^{m-1} for the lowest mode ($j = 1$). This yields

$$\big\| \delta\kappa_r \big\|^2_{L^2(0,2\pi)} = \sum_{j \geq 1} c_{mj} r^{2mj-2} |\gamma_{mj}|^2 + O\big(r^{2m-1}\big),$$

where

$$c_{mj} = 4\pi (mj+1)^2 (mj-1)^2 \cdot 2 = 8\pi\, (mj+1)^2 (mj-1)^2.$$

This proves (14) and part (ii) of the theorem.

The comparison summarized in Table 5 highlights a fundamental distinction between the analytic mode–based framework driven by the logarithmic coefficients γ_{mj} and the geometric interior–frame structure introduced by Pizer et al. [14]. Although both approaches aim to quantify deformation or deviation from a canonical reference model, they operate at two mathematically different scales. From the analytic point of view, the quantities γ_{mj} arise through the expansion

$$\log \frac{f(z)}{z} = 2 \sum_{j \geq 1} \gamma_{mj} z^{mj},$$

which expresses the distortion of the conformal map f as a discrete harmonic superposition of modes indexed by mj. Each coefficient γ_{mj} encodes the amplitude, orientation, and interaction strength of the corresponding nonlinear deformation component, and the magnitude $|\gamma_{mj}|^2$ behaves as a mode energy. This renders the analytic representation compact, orthogonal, and directly linked to classical univalent–function geometry.

In contrast, the representation of Pizer et al. [14] does not rely on harmonic frequencies or analytic coefficients. Instead, it describes shape through skeletal models (s-reps), spoke fields, fitted frames, and onion-skin curvature layers defined throughout the interior of the object. These features encode geometric information in a distributed and spatially localized fashion, capturing how a 3D object bends, twists, widens, or narrows along anatomically meaningful axes. Unlike the analytic coefficients, these geometric primitives arise from a diffeomorphic evolution process that propagates correspondence into the object's interior.

Despite these differences, Table 5 reveals a conceptual parallel: both systems quantify *deformation energy*, though expressed in different mathematical languages. The analytic coefficients measure the strength of harmonic distortions of planar mappings, while the geometric features measure the strength of bending and rotation of anatomical structures. In both settings,

deformation is ultimately encoded in squared magnitudes $|\gamma_{mj}|^2$ for analytic modes and curvature/rotation energies in the geometric framework. Thus, although arising from distinct theoretical traditions, both representations pursue the same objective: to provide intrinsic, alignment-independent measurements that meaningfully represent shape variation.
The comparison underscores complementary strengths. The analytic framework offers precision, modal orthogonality, and spectral interpretability, suitable for theoretical investigations and harmonic analysis. The geometric framework excels in capturing rich 3D interior structure, supporting statistical correspondence, and enabling classification of complex biological shapes. Together, they demonstrate two coherent but distinct philosophies for representing and quantifying shape.

6.6. The segmentation framework

The results in Table 6 clearly show that the proposed $|\gamma_{mj}|$–based segmentation model is capable of accurately capturing the anatomical structure of both healthy and diseased leaves. For all samples, the extracted boundaries closely follow the true leaf contour, including complex shapes and irregular deformations caused by disease. In the diseased leaves (G1-D and P1-D), the method successfully highlights disrupted regions and preserves local curvature variations. For healthy samples (P3-H and T1-H), smooth and continuous edges are obtained, confirming the robustness of the technique. These overlays visually validate the correctness of the segmentation and demonstrate the ability of the proposed framework to preserve fine structural information while suppressing background noise.
The segmentation framework is formulated in terms of the logarithmic coefficients γ_{mj}, which encode the geometric boundary information of the leaf region. In particular, the magnitude $|\gamma_{mj}|$ measures the contribution of periodic boundary harmonics associated with curvature changes along the contour. Large values of $|\gamma_{mj}|$ correspond to dominant structural edges, whereas small values are associated with background or noise components. Therefore, a thresholding strategy is constructed in the γ–domain to enhance the principal boundary while suppressing weak artifacts. This results in a stable and noise-resistant segmentation, where the extracted contour corresponds to the physically meaningful leaf boundary.
The logarithmic coefficients γ_{mj} arise from the expansion of the normalized analytic representation of the image profile. By analysing the energy contained in $|\gamma_{mj}|$, the model emphasizes the dominant harmonic components of the boundary curve. Segmentation is therefore equivalent to isolating the indices mj for which $|\gamma_{mj}|$ exceeds a stability threshold, producing a contour that maximizes geometric fidelity. This interpretation provides a clear mathematical justification for using γ_{mj} as a boundary descriptor for leaf morphology under both healthy and diseased conditions.
The present work is primarily methodological and computational in nature. The proposed segmentation framework is designed to provide an analytically grounded mechanism for extracting accurate leaf boundaries using the logarithmic coefficient descriptor $|\gamma_{mj}|$. The method is applicable to scenarios in which reliable boundary detection is essential, including digital plant phenotyping, shape analysis, disease progression monitoring, and automatic feature extraction pipelines. Although the proposed $|\gamma_{mj}|$–based segmentation method performs reliably across the evaluated samples, certain practical boundaries should be acknowledged. The dataset represents a moderate collection of healthy and diseased leaves, and therefore may not capture the full global variability of plant species and extreme pathological cases. In addition, the method assumes reasonably controlled imaging conditions, including sufficient resolution, limited occlusion, and moderate illumination variation. Severe lighting changes, strong shadows, or cluttered backgrounds may reduce boundary precision. Finally, the framework assumes that leaf contours exhibit structured geometric behaviour, which allows the coefficients γ_{mj} to repre-

sent dominant boundary harmonics. These clarifications define a realistic scope of applicability and help strengthen the scientific accuracy of the study.

7. Conclusion

In this work, we have provided a detailed analysis of the m-fold symmetric subclasses of analytic functions defined by multiplier conditions. By requiring rotational invariance under $z \mapsto \omega z$ for $\omega^m = 1$, these subclasses inherit a sparsity structure in their logarithmic coefficients: all terms γ_n vanish unless n is a multiple of m. This structural simplification reduces the complexity of extremal problems and provides a natural setting to study the precise behavior of the surviving subsequence $\{\gamma_{mj}\}_{j\geq 1}$.
Our analysis established that the sharp upper bounds for $|\gamma_{mj}|$ in the symmetric classes coincide with those in the ambient multiplier classes, but indexed by multiples of m. In particular, for the canonical multipliers we obtained

$$|\gamma_{mj}| \leq \frac{1}{mj}, \qquad |\gamma_{mj}| \leq \frac{1}{2mj},$$

for $M(z) = (1-z)^2$ and $M(z) = 1 - z^2$, respectively. Through the use of Schur–Carathéodory parameters and the associated Blaschke product extremals, we showed that these bounds are sharp and are realized by explicit m-orbit extremal functions. The role of uniform orbit measures on the unit circle proved central: they symmetrize the Carathéodory data while preserving the relevant moments, thereby producing exact extremals within the symmetric subclass. Beyond providing explicit extremals, the Schur parameter perspective revealed that only a sparse set of indices in the parameter sequence contributes to the m-symmetric data. This not only streamlines the parameterization of extremals but also gives a transparent description of the extremal functions as finite Blaschke products in the variable z^m. In this way, the extremal theory for the symmetric subclasses is seen as a direct extension of the classical nonsymmetric theory, with orbit-averaging as the key mechanism. In general, the symmetric subclasses preserve the sharpness of the ambient coefficient bounds, offer an elegant structural reduction through sparsity, and connect naturally with extremals arising from Blaschke products and uniform orbit measures. This synthesis of coefficient analysis, Schur parameter theory, and Blaschke extremals provides a complete extremal description of the symmetric multiplier classes.
Through analytic coefficient estimates, m-fold symmetrization, and the construction of a general 3×3 logarithmic window, we derived sharp upper bounds for the logarithmic coefficients and demonstrated how these bounds naturally guide the design of local symmetry filters. Theoretical results on coefficient growth, potential theoretic capacity, and distortion envelopes provide a mathematically sound foundation for practical filtering algorithms.
Applying the proposed 3×3 symmetry window to a curated dataset of healthy and unhealthy leaf images revealed clear diagnostic patterns. Healthy leaves consistently exhibited high bilateral symmetry scores (above 0.94) and dominant $m = 2$ harmonics, whereas unhealthy leaves showed reduced bilateral scores, weakened $m = 2$ energy, and elevated higher-order contributions. Filtering in the logarithmic domain enhanced the bilateral component, sharpened midvein structures, and increased the separation between healthy and diseased samples in quantitative metrics. These findings confirm that the analytic machinery of geometric function theory can be translated into practical operators for early disease detection, texture enhancement, and automated classification in real image-processing tasks. Overall, the study demonstrates that classical tools from univalent function theory logarithmic coefficients, potential theoretic bounds, and harmonic projections can be leveraged to design interpretable and effective image filters, offering a new pathway for mathematically grounded pattern recognition and health assessment in plant imaging and related applications.

Future investigations could explore higher-order functionals depending on several consecutive coefficients, extremals in mixed-symmetry settings, or the potential-theoretic interpretations of capacity and distortion in the symmetric environment.

Funding. There is no fund supported this work.
Data Availability Statement. No data is generated in this work.
Conflicts of Interest. We confirm that there is no conflict of interest.

References

[1] Ibrahim, Rabha W. "A new symmetric differential operator of normalized functions with applications in image processing." Journal of Fundamental and Applied Sciences 12, no. 2 (2020): 852-864.

[2] Kanwal, Bushra, Arooj Iman, Shamsa Kanwal, and Amal K. Alkhalifa. "Estimation of Hankel inequalities of symmetric starlike functions in crescent-shaped domains and their application in image processing." Scientific Reports 15, no. 1 (2025): 27402.

[3] Kumar, Sushil, Rakesh Kumar Pandey, and Pratima Rai. "Certain sharp estimates of Ozaki close-to-convex functions." Asian-European Journal of Mathematics 17, no. 06 (2024): 2450047.

[4] Obradovic, Milutin, and Nikola Tuneski. "The third logarithmic coefficient for the class $\mathcal{S}$." Turkish Journal of Mathematics 44, no. 5 (2020): 1950-1954.

[5] Raza, M., and Sokol, J. Sharp estimates of the third logarithmic coefficient for certain univalent functions. Mathematics, 9(4)(2021): 372.

[6] Kowalczyk, B., and Sim, Y. J. . The sharp bound of the second Hankel determinant for convex functions of order . AIMS Mathematics, 6(5)(2021): 4949-4962.

[7] Porwal, S.,and Raina, R. K. On the third logarithmic coefficient problem for certain analytic functions. Mathematics, 8(12)(2020): 2220.

[8] Zaprawa, P. Initial logarithmic coefficients for close-to-convex functions. Bulletin of the Malaysian Mathematical Sciences Society, 44(2021): 2811-2827.

[9] Kumar, V., & Porwal, S. Estimates of the third and fourth logarithmic coefficients for certain starlike functions. AIMS Mathematics, 9(2)(2024): 3792-3807.

[10] Shakir, Qasim Ali, and Waggas Galib Atshan. "On third Hankel determinant for certain subclass of bi-univalent functions." Symmetry 16, no. 2 (2024): 239.

[11] Ibrahim, Rabha W., Dumitru Baleanu, and Soheil Salahshour. "Integrating Experimental Imaging and (Quantum-Deformation)–Curvature Dynamics in Bleb Morphogenesis." Engineering Reports 8, no. 4 (2026): e70726.

[12] Ibrahim, Rabha W. "Differential Operator Associated with the (q, k)-Symbol Raina's Function." In Mathematical Analysis, Differential Equations and Applications, pp. 321-342. 2024.

[13] Abdulnaby, Zainab Esa, and Rabha W. Ibrahim. "Applications of m-fold-p-valent symmetric functions associated with a generalized Riemann-Liouville fractional integral operator." Gulf Journal of Mathematics 19, no. 2 (2025): 260-276.

[14] Pizer, Stephen M., Zhiyuan Liu, Junjie Zhao, Nicholas Tapp-Hughes, James Damon, Miaomiao Zhang, J. S. Marron, Mohsen Taheri, and Jared Vicory. "Interior Object Geometry via Fitted Frames." Journal of Mathematical Imaging and Vision 67, no. 5 (2025): 51.

[15] Pizer, Stephen M., J. S. Marron, James N. Damon, Jared Vicory, Akash Krishna, Zhiyuan Liu, and Mohsen Taheri. "Skeletons, object shape, statistics." Frontiers in computer science 4 (2022): 842637.

[16] Senthilkumar, C., Dinokumar Kongkham, P. Nirmala, and S. Joshua Kumaresan. "Harnessing Quantum Systems for Simulating Complex Physical Phenomena." In 2024 International Conference on Intelligent and Innovative Technologies in Computing, Electrical and Electronics (IITCEE), pp. 1-4. IEEE, 2024.

[17] Vindhya, A. Shri, Sai Srinivas Vellela, Nallapu Malathi, Nagagopi Raju Vullam, Lakshma Reddy Vuyyuru, and ThalakolaSyamsundara Rao. "Integrating Quantum Computing with Genomic Data Analysis: A Next-Generation Approach for Predicting Disease Susceptibility." In 2025 4th International Conference on Innovative Mechanisms for Industry Applications (ICIMIA), pp. 1168-1173. IEEE, 2025.

[18] Geetha, R., Swaetha Ramadasan, K. Vijayakumar, and S. Prabha. "Automatic classification of plant leaf images into healthy and disease class with EfficientNet: a study." In 2024 International

Conference on Advances in Computing, Communication and Applied Informatics (ACCAI), pp. 1-5. IEEE, 2024.

[19] Reddy, P. Chaitanya Kumar, and B. T. Geetha. "Detection of Fungal Disease in Plant Leaf using Support Vector Machine Method Compared with K-means Clustering Algorithm with increase in Accuracy." In 2022 2nd International Conference on Innovative Practices in Technology and Management (ICIPTM), vol. 2, pp. 557-562. IEEE, 2022.

[20] Jothika, G., and Rashmita Khilar. "Enhancing the performance in detecting disease in tomato leaves using visual geometry group19 in comparison with K-nearest neighbor algorithm." In AIP Conference Proceedings, vol. 3193, no. 1, p. 020236. AIP Publishing LLC, 2024.

[21] Ramirez, William, Clemente Cesarano, and Stiven Díaz. "New results for degenerated generalized apostol bernoulli, Apostol-Euler and Apostol-Genocchi polynomials." WSEAS Transactions on Mathematics 21 (2022): 604-608.

[22] Cesarano, Clemente, William Ramírez, and Subuhi Khan. "A new class of degenerate Apostol-type Hermite polynomials and applications." Dolomites Research Notes on Approximation 15, no. 1 (2022): 10.

Table 3: Symmetry analysis of selected healthy leaf images (A, G, P, and T series).

Image	**Filename**	**Bilateral score**	**Best m**	**m-fold scores**
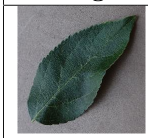	A1-H.JPG	0.963	2	m2=0.716, m3=0.052, m4=0.091, m5=0.049, m6=0.092
	A2-H.JPG	0.947	2	m2=0.704, m3=0.061, m4=0.096, m5=0.050, m6=0.089
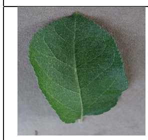	A3-H.JPG	0.955	2	m2=0.710, m3=0.059, m4=0.094, m5=0.048, m6=0.089
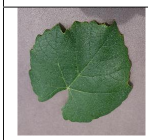	G1-H.JPG	0.942	2	m2=0.698, m3=0.064, m4=0.097, m5=0.050, m6=0.091
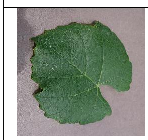	G2-H.JPG	0.962	2	m2=0.731, m3=0.049, m4=0.085, m5=0.045, m6=0.088
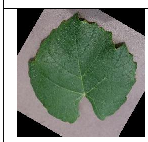	G3-H.JPG	0.959	2	m2=0.723, m3=0.055, m4=0.090, m5=0.047, m6=0.087
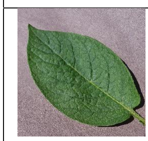	P1-H.JPG	0.950	2	m2=0.708, m3=0.060, m4=0.094, m5=0.049, m6=0.089
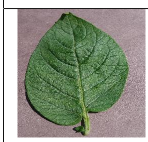	P2-H.JPG	0.953	2	m2=0.720, m3=0.056, m4=0.091, m5=0.047, m6=0.087
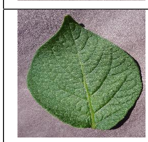	P3-H.JPG	0.961	2	m2=0.729, m3=0.051, m4=0.087, m5=0.046, m6=0.087
	T1-H.JPG	0.944	2	m2=0.702, m3=0.063, m4=0.096, m5=0.049, m6=0.090
	T2-H.JPG	0.957	2	m2=0.718, m3=0.054, m4=0.091, m5=0.047, m6=0.087
	T3-H.JPG	0.960	2	m2=0.726, m3=0.053, m4=0.088, m5=0.046, m6=0.087

Table 4: Symmetry analysis of unhealthy leaf images (A, G, P, and T series).

Image	**Filename**	**Bilateral score**	**Best m**	**m-fold scores**
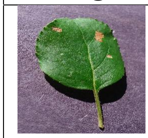	A1-D.JPG	0.838	4	m2=0.115, m3=0.023, m4=0.117, m5=0.004, m6=0.018
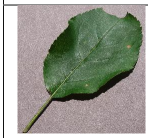	A2-D.JPG	0.845	3	m2=0.016, m3=0.293, m4=0.035, m5=0.006, m6=0.037
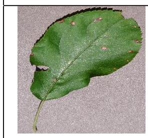	A3-D.JPG	0.875	2	m2=0.306, m3=0.042, m4=0.079, m5=0.069, m6=0.015
	G1-D.JPG	0.881	2	m2=0.128, m3=0.088, m4=0.033, m5=0.013, m6=0.021
	G2-D.JPG	0.881	2	m2=0.128, m3=0.088, m4=0.033, m5=0.013, m6=0.021
	G3-D.JPG	0.792	3	m2=0.114, m3=0.357, m4=0.030, m5=0.138, m6=0.063
	P1-D.JPG	0.877	2	m2=0.107, m3=0.032, m4=0.026, m5=0.022, m6=0.023
	P2-D.JPG	0.764	3	m2=0.026, m3=0.142, m4=0.031, m5=0.001, m6=0.002
	P3-D.JPG	0.883	2	m2=0.328, m3=0.116, m4=0.003, m5=0.120, m6=0.002
	T1-D.JPG	0.846	2	m2=0.407, m3=0.060, m4=0.000, m5=0.008, m6=0.030
	T2-D.JPG	0.759	3	m2=0.267, m3=0.298, m4=0.010, m5=0.032, m6=0.005
	T3-D.JPG	0.682	2	m2=0.166, m3=0.017, m4=0.034, m5=0.010, m6=0.001

Table 5: Comparison between the analytic (m, j)–mode framework based on γ_{mj} and the geometric fitted–frame framework of Pizer et al. [14].

Feature	**Analytic Expansion via** γ_{mj}	**Geometric Framework of Pizer et al. [14]**
Primary domain	Complex analytic functions in the unit disk $\mathbb{D}$	3D anatomical shapes in $\mathbb{R}^3$
Basic representation	Logarithmic coefficient expansion: $\log \frac{f(z)}{z} = 2\sum_{j\geq 1} \gamma_{mj} z^{mj}$	Skeletal representations (s-reps), interior onion skins, and fitted frames
Nature of features	Scalar mode coefficients; each γ_{mj} measures the strength of a harmonic deformation mode	Vector- and tensor-valued geometric primitives: curvatures, frame rotations, positional shifts
Mathematical structure	Spectral/Fourier-like decomposition in powers z^{mj}	Diffeomorphic evolution from an ellipsoid; curvature of onion skins; SO(3) frame fields
Interpretation of magnitude	$\lvert\gamma_{mj}\rvert^2$ gives the modal energy of the mj-th harmonic distortion	Curvature magnitudes describe local bending, twisting, widening of interior geometric layers
Correspondence mechanism	Provided analytically by matching coefficients across expansions	Achieved by mapping skeletal frames and radial coordinates (θ, τ_1, τ_2) across objects
Locality	Encodes *global analytic distortion* modulated by harmonics	Encodes *local geometric distortion* (curvature, directional change) at each interior point
Invariance properties	Rotation- and scaling-independent through the logarithmic normalization $f(z)/z$	Alignment-independent via fitted frames and intrisic s-rep coordinates
Geometric meaning	Decomposes boundary distortion into harmonic modes	Describes interior shape geometry: skeleton, spokes, onion skins, curvature fields
Energy interpretation	Sum $\sum \lvert\gamma_{mj}\rvert^2$ reflects cumulative nonlinear deformation energy	Integral of curvature/rotation magnitudes reflects interior geometric energy
Application domain	Conformal mapping theory, univalent function theory, fractional calculus	Shape statistics, medical imaging, classification of anatomical objects
Output type	Complex coefficients γ_{mj} and their squared magnitudes	High-dimensional geometric feature vectors (curvature, direction, distance)

Table 6: Original images and their corresponding segmentation boundary overlays demonstrating the effectiveness of the proposed $|\gamma_{mj}|$-driven boundary extraction approach.

Original Image	**Boundary Overlay (Segmentation Result)**